RSC Advances

REVIEW

View Article Online
View Journal | View Issue

Cite this: *RSC Adv.*, 2023, **13**, 27333

Recent theranostic applications of hydrogen peroxide-responsive nanomaterials for multiple diseases

Linjie Huang, Yina Su, Dongdong Zhang, Zheng Zeng, Xueqi Hu, Shanni Hong* and Xiahui Lin *

Received 25th July 2023
Accepted 31st August 2023

DOI: 10.1039/d3ra05020c

rsc.li/rsc-advances

It is well established that hydrogen peroxide (H_2O_2) is associated with the initiation and progression of many diseases. With the rapid development of nanotechnology, the diagnosis and treatment of those diseases could be realized through a variety of H_2O_2-responsive nanomaterials. In order to broaden the application prospects of H_2O_2-responsive nanomaterials and promote their development, understanding and summarizing the design and application fields of such materials has attracted much attention. This review provides a comprehensive summary of the types of H_2O_2-responsive nanomaterials including organic, inorganic and organic-inorganic hybrids in recent years, and focused on their specific design and applications. Based on the type of disease, such as tumors, bacteria, dental diseases, inflammation, cardiovascular diseases, bone injury and so on, key examples for above disease imaging diagnosis and therapy strategies are introduced. In addition, current challenges and the outlook of H_2O_2-responsive nanomaterials are also discussed. This review aims to stimulate the potential of H_2O_2-responsive nanomaterials and provide new application ideas for various functional nanomaterials related to H_2O_2.

1 Introduction

As a biomolecule, hydrogen peroxide (H_2O_2) is commonly generated from specifically triggered enzymatic systems and cellular metabolism, and has been linked to the development and progression of multiple diseases.[1–6] Overexpression of H_2O_2 is a typical feature of the microenvironment in numerous diseases.[7,8] It can be catalyzed to produce significant substances, including oxygen (O_2) and hydroxyl radicals ($^{\bullet}OH$). The O_2 not only alleviates the hypoxic environment of some diseases such as tumors and inflammation, but also can be converted into singlet oxygen to kill bad cells.[9–11] The $^{\bullet}OH$ as a type of reactive oxygen species (ROS) can cause the oxidative stress of cells, which could be beneficial in treating tumors and bacterial infections.[10] However, the ability of H_2O_2 also is a double-edged sword and poses a risk in certain conditions.[12,13] Excessive H_2O_2 induced DNA damage and protein denaturation, resulting in mutations and genetic instability.[11] It is unfavorable to the treatment of diseases, such as inflammation, bone injury, cardiovascular diseases, and so on. By observing the changes of H_2O_2 concentration in the lesion, the corresponding physiological and pathological state of the lesion could be detected.[14] Therefore, there should be different choices for catalyzing or consuming H_2O_2 based on different disease types.

With the development of nanotechnology, a growing number of H_2O_2-responsive nanomaterials have been designed and investigated for biomedical applications. H_2O_2-responsive nanomaterials can be simply classified as organic, inorganic, and hybrid nanomaterials. In particular, the core components of H_2O_2-responsive organic nanomaterials mainly are organic molecules and enzymes.[15–18] For example, some organic molecules react with H_2O_2 causing the changes of their absorption or emission characteristics, such as 2,2′-azino-bis(3-ethylbenzothiazoline-6-sulfonic acid) (ABTS).[3,19] Some enzymes like catalase (CAT) were applied for decomposing H_2O_2, producing O_2 and water.[16–18,20,21] Compared to organic nanomaterials, inorganic H_2O_2-responsive nanomaterials have greater stability, more functionalities, and a broader range of applications. There inorganic nanomaterials with enzyme-like properties, such as metal oxides and noble metal nanoparticles, were utilized to react with H_2O_2.[22,23] According to the composition of inorganic nanomaterials, the reaction products can be broadly classified as metal ions, O_2 or ROS, *etc.* And some hybrid nanomaterials formed by the combination of organic and inorganic materials combine their respective advantages and play an important role in H_2O_2-related applications.[24,25]

For therapeutic applications, H_2O_2-responsive nanomaterials provided a variety of treatment methods, mainly including producing ROS and consuming H_2O_2.[10,26–30] These nanomaterials employ their characteristics to participate in the treatment of many diseases, including tumors, bacteria,

School of Medical Imaging, Fujian Medical University, Fuzhou 350122, Fujian, P. R. China. E-mail: xiahuilin@fjmu.edu.cn; snhong2020@fjmu.edu.cn

inflammation, cardiovascular diseases, bones, neurologic diseases and ophthalmic diseases.[26,27,31,32] For tumors and bacterial infections, decomposing or catalyzing H_2O_2 often generates other ROS to enhance the treatment effect, while for other diseases such as inflammation, it's crucial to eliminate the oxidative stress of H_2O_2 to foster injury repair and maintain normal physiological state.[10,26–30,33] The research focused on the elimination of H_2O_2 has also been applied for the treatment of diseases such as inflammation, uveitis, and ischemic stroke.[34–36] Furthermore, H_2O_2-related diagnosis based on H_2O_2-responsive nanomaterials holds promise for the diagnosis of multiple diseases *via* medical imaging technology like fluorescent imaging (FLI), photoacoustic imaging (PAI), ultrasound (US) imaging, and magnetic resonance imaging (MRI).[37–40] For example, the catalytic decomposition of H_2O_2 produces O_2 bubbles that reflect ultrasound signals in US imaging.[41] Another example, the conversion of ABTS into oxidized ABTS in the presence of H_2O_2 leads to strong near-infrared (NIR) absorbance, thus used for PA imaging.[42] The combination of H_2O_2-responsive nanomaterials and imaging technology provides a new avenue for disease diagnosis. As more diseases are found to be closely related to H_2O_2, understanding the working principle of H_2O_2-responsive nanomaterials and developing novel and efficient theranostic reagents will unlock additional application channels of H_2O_2-responsive nanomaterials and help address various diseases.

This review summarizes recent advancements in the treatment and imaging of partial diseases associated with H_2O_2, including the design of H_2O_2-responsive nanomaterials and application strategies for different diseases (Fig. 1). The mechanisms and functions of various types of H_2O_2-responsive nanomaterials in the treatment of different diseases are also discussed and summarized. Furthermore, therapeutic applications utilizing H_2O_2-responsive nanomaterials are categorized into two different groups: (1) producing ROS and (2) consuming H_2O_2. The former included tumors, bacterium, dental diseases. The latter included inflammations, cardiovascular diseases, bones, neurologic diseases and ophthalmic diseases. The diagnosis agents that are based on H_2O_2-responsive nanomaterials are utilized for diagnosis purposes in four categories: fluorescence imaging, photoacoustic imaging, ultrasonic imaging, and magnetic resonance imaging. The purpose of this review is to integrate recent

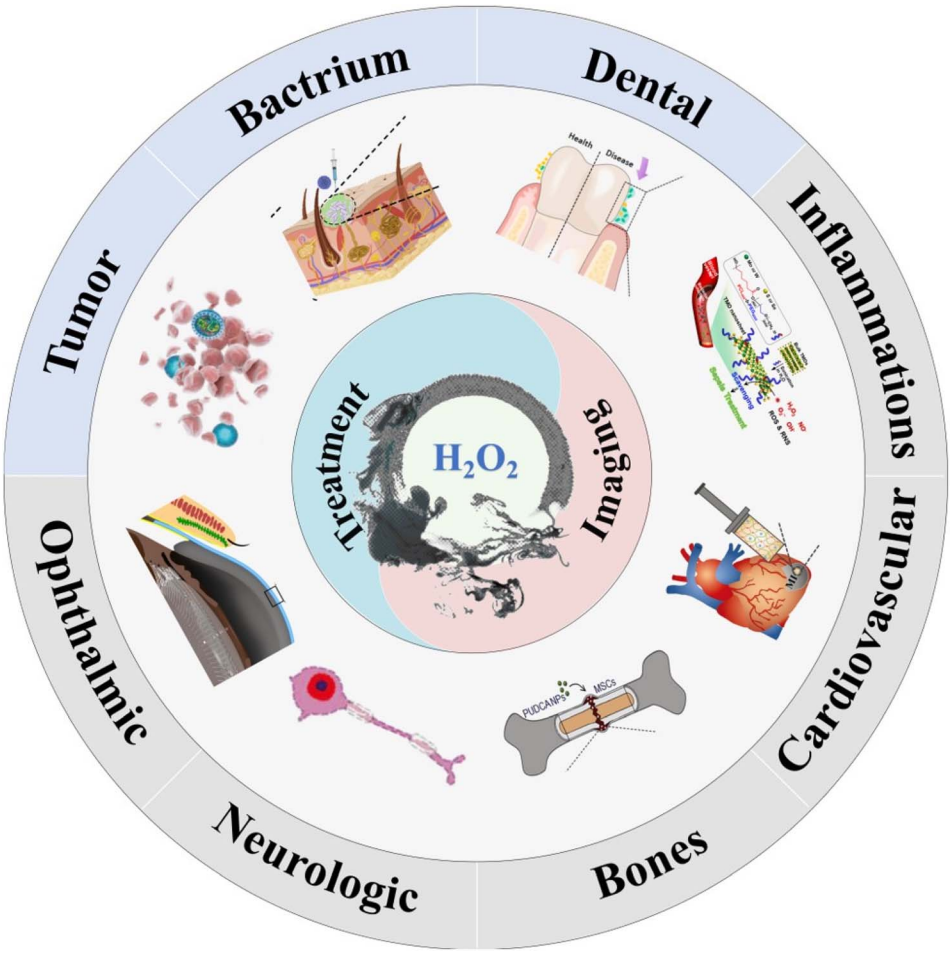

Fig. 1 Theranostic applications of H_2O_2-responsive nanomaterials, including tumors, bacterium, dental diseases, inflammations, cardiovascular diseases, bones, neurologic diseases, and ophthalmic diseases.

Table 1 Categorization of H_2O_2-responsive nanomaterials in recent years

Category		Material	Mechanism	Mode	Ref.
Organic nanomaterials	Small molecules	BSA-MBPB	Boron-carbon link	Releasing drug	Zeng *et al.*[47]
		BODIPY-based photosensitizer	Arylboronate group	Recovering fluorescence	Wang *et al.*[48]
		PF1	Boric acid	Detecting H_2O_2	Chang *et al.*[49]
		Diselenide based cross-linker nanomaterial	Diselenide bridges	Releasing DOX	Jo *et al.*[51]
		HKPerox-1 and HKPerox-2	Payne/Dakin reaction	Molecular recognition of H_2O_2	Ye *et al.*[54]
		DPPEA-HC	Reaction of triphenylphosphine	Detecting H_2O_2	Soh *et al.*[56]
		ABTS	Oxidation reaction	Photoacoustic imaging	Ding *et al.*[57]
	Enzymes	HA-CAT@aCe6	Catalase	Producing O_2	Phua *et al.*[63]
		PLGA-R837@Cat	Catalase	Relieving the tumor hypoxia	Chen *et al.*[64]
	Organic polymer nanoparticles	PVAX polymer nanoparticles	Peroxalate ester linkages	Decreasing H_2O_2 and releasing drug	Park *et al.*[66]
		POD-PEG NPs	Oxalate ester bond	Releasing drug	Ou *et al.*[67]
		Block copolymer NPs	Change of particle size	Releasing drug	Phan *et al.*[65]
		SCNPs	Heavy-atom effect	Detecting H_2O_2	Lu *et al.*[68]
		Metalloporphyrin-based porous organic polymer	POD-like activity	Detecting H_2O_2	Liu *et al.*[69]
	Hydrogels	Hydrogel based on the thiazolidinone group	Gel–sol phase transition	Releasing drug	Ren *et al.*[71]
		L012@PAni-PAAm hydrogels	Biosensors	Monitoring H_2O_2	Guo *et al.*[72]
Inorganic nanomaterials	Metal oxides	MnO_2@PtCo nanoflowers	Catalase mimic	Relieving hypoxic condition	Wang *et al.*[81]
		IR780-sMnO_2-PCM NPs	Catalase mimic	Producing O_2	Zhang *et al.*[82]
		Co_3O_4 NPs	Oxidase mimic and peroxidase mimic	Detecting H_2O_2	Zhang *et al.*[85]
	Metal ions	H–MnO_2@TPyP@Bro	Generating $^{\bullet}OH$ by Mn^{2+}	Chemodynamic therapy	Zhu *et al.*[90]
		Fe(III)@WS2-PVP NPs	Fenton reation	Chemodynamic therapy	Wu *et al.*[91]
	Single-atom enzyme	Fe-SANzyme nanozymes	Catalase-like activity	Producing O_2	Zhang *et al.*[96]
		Pd-based SAzyme	POD mimic	Generation of $^{\bullet}OH$	Zhu *et al.*[97]
	Noble metal nanoparticles	SiO_2–Pt	CAT mimic	Producing O_2	Lyn *et al.*[104]
		Ru nanoframes	POD mimic	Generation of $^{\bullet}OH$	Ye *et al.*[107]
Hybrid nanomaterials	Metal–organic frameworks	ICG@Mn/Cu/Zn-MOF@MnO_2	Producing $^{\bullet}OH$ by Cu^{+} and Mn^{2+}	CDT	Cheng *et al.*[24]
		GOx@ZIF@MPN	Producing $^{\bullet}OH$ by Fe^{2+}	CDT	Zhang *et al.*[113]
	Quantum dots and their capping agents or coating	MPA capped CdTe QDs	Fluorescence signal change	Detecting H_2O_2	Castro *et al.*[115]
		Si–CdTe hybrid QDs	Cd–S bond	Detecting H_2O_2	Zhou *et al.*[116]
		Cy5-labeled HRP–QDs	Fluorescence change	Detecting H_2O_2	Huang *et al.*[118]
	Noble-metal nanoclusters and organic protective agents	AgNCs protecting BSA	Dual-emission fluorescent	Detecting H_2O_2	Chen *et al.*[120]
		AgNCs protecting [C4py][124]	Coordination bond between AsO_3^{3-} and π molecular orbitals	Detecting H_2O_2	Wang *et al.*[121]

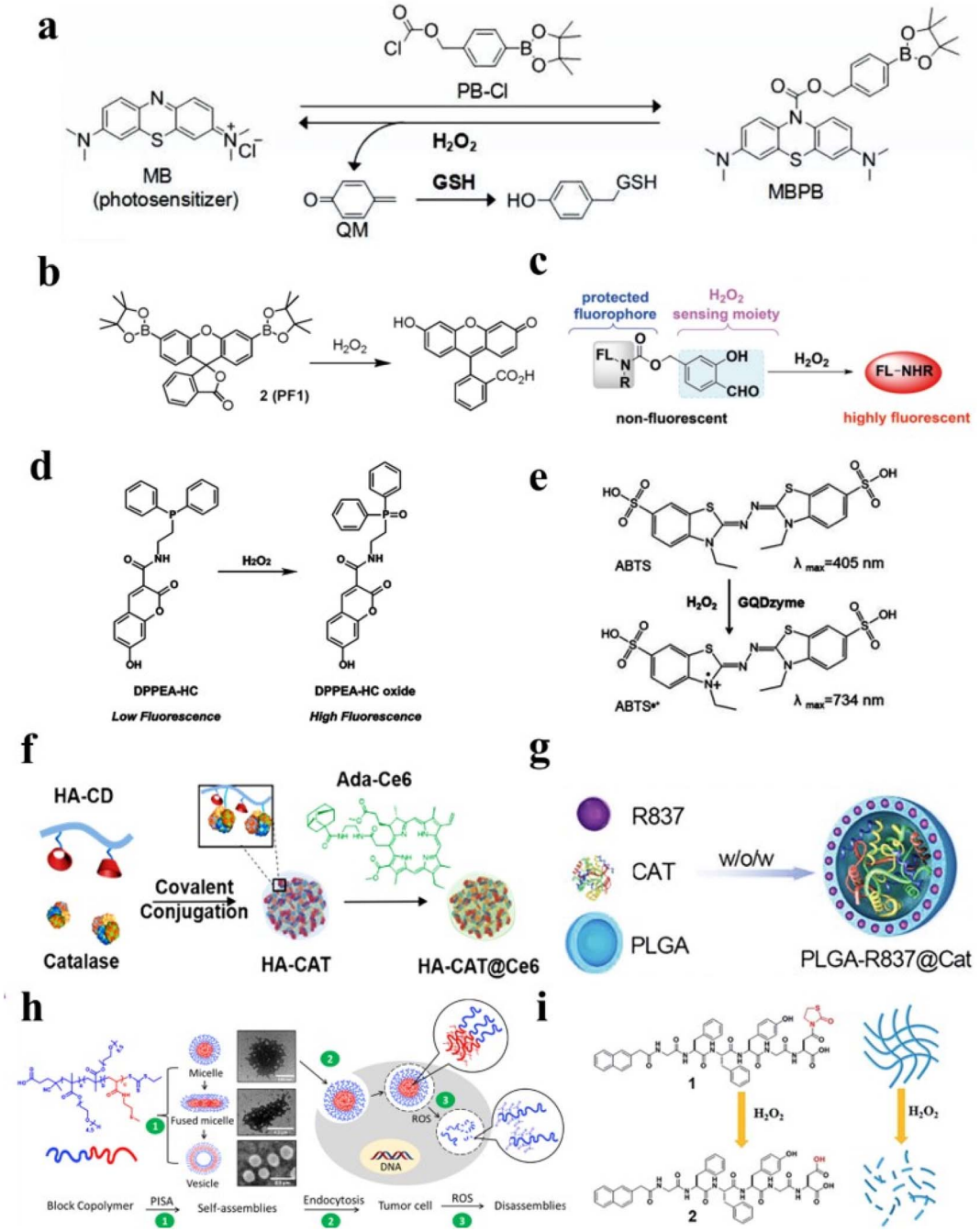

Fig. 2 (a) A schematic diagram illustrating of MBPB to deliver methylene blue. Reproduced from ref. 47 copyright 2019, Elsevier Ltd. (b) A schematic diagram illustrating H_2O_2-related fluorescent conversion of PF1. Reproduced from ref. 49 copyright 2004, American Chemical Society. (c) Schematic of a tandem Payne/Dakin reaction. Reproduced from ref. 54 copyright 2018, Wiley-VCH Verlag GmbH & Co. KGaA, Weinheim. (d) A schematic diagram illustrating the fluorescence intensity of DPPEA-HC enhanced. Reproduced from ref. 56 copyright 2004, Elsevier Ltd. (e) A schematic diagram illustrating the conversion of ABTS in the presence of H_2O_2. Reproduced from ref. 57 copyright 2019, American Chemical Society. (f) The preparation process of HA-CAT@Ce6 by the conjugation of HA with CAT. Reproduced from ref. 63 copyright 2019, American Chemical Society. (g) Schematic of PLGA to encapsulate CAT. Reproduced from ref. 64 copyright 2019, WILEY-VCH Verlag GmbH & Co. KGaA, Weinheim. (h) Schematic of the evolution of particle size and morphology of H_2O_2-sensitive block copolymer NPs. Reproduced from ref. 65 copyright 2022, American Chemical Society. (i) Schematic of releasing drugs *via* H_2O_2-responsive hydrogels. Reproduced under terms of the CC-BY license.[71] Copyright 2017, Chunhua Ren, published by RSC Advances.

findings on H_2O_2-related diseases and H_2O_2-responsive nanomaterials, and to advance the field of H_2O_2-related biomedicine. These strategies and studies allow for better understanding of the functions and mechanisms of H_2O_2-responsive nanomaterials and also open up more possibilities for other biomedical application scenarios.

2 H_2O_2-responsive nanomaterials

In this section, the H_2O_2-responsive nanomaterials are introduced that came in three forms (Table 1): organic nanomaterials, inorganic nanomaterials, and hybrid nanomaterials.

2.1 H_2O_2-responsive organic nanomaterials

Organic nanomaterials possess unique advantages, such as biosafety and easy synthesis. We summarize some H_2O_2-responsive organic nanomaterials, including small molecules, enzymes, organic polymer nanoparticles and hydrogels.

2.1.1 Small molecules

2.1.1.1 Boronate-based small molecules. Recently, boronate-based molecules have been reported as H_2O_2-responsive organic molecules, which can be selectively hydrolyzed by H_2O_2.[15] Its reaction with H_2O_2 was mainly based on the cleavage of the formed boron-carbon link.[43] Boronate-based organic nanoparticles were widely used in the biomedical field, including H_2O_2-responsive drug delivery and detection.[44–46]

For example, Zeng *et al.* designed a pro-photosensitizer MBPB based on boron-carbon link, which could be hydrolyzed by H_2O_2 and achieved responsive release of methylene blue (MB) and quinone methide (QM) in Fig. 2a.[47] After being ingested by tumor cells, the MBPB under the activation of H_2O_2 would release MB to produce $^1O_2$ and QM to enhance oxidative stress, and finally play a role in enhancing photodynamic therapy. Moreover, Wang *et al.* designed a H_2O_2-responsive photosensitizer contained a diiodo distyryl boron dipyrromethene (BODIPY) core and an arylboronate group, which quenched the fluorescence signal of BODIPY by photoinduced electron transfer (PET).[48] The arylboronate group did not break without H_2O_2, and the fluorescence of PET was still inhibited. However, in the presence of H_2O_2, the strong fluorescence emission would be produced by BODIPY. Herein, the combination of arylboronate group and BODIPY as H_2O_2-responsive fluorescence nanomaterials had enormous potential. Chang and coworkers reported a peroxyfluor-1 (PF1) molecule which could be used for detecting H_2O_2 in living cells *via* fluorescence signals change (Fig. 2b).[49] PF1 used the boric acid deprotection mechanism to detect H_2O_2 in aqueous solutions of reactive oxygen species, providing an unprecedented selectivity and optical dynamic range.

2.1.1.2 H_2O_2-responsive diselenide bridges. Similar to the B–C link, the diselenide bridge could be also cleaved by H_2O_2.[50] Based on this, H_2O_2-responsive diselenide bridges were often used for controllable drug delivery. For example, Jo *et al.* designed H_2O_2-stimuli responsive nanomaterials based on diselenide bridges, which showed a rapid release of doxorubicin (DOX) in the presence of H_2O_2.[51] The diselenide bridge could be cleaved and converted to seleninic acid, providing a good direction for biomedical research.[52] Not only that, some selenide-based nanoparticles can produce fluorescence *via* the oxidation of H_2O_2.[53]

2.1.1.3 Other small molecules. In addition, some molecules can also serve as probes to achieve H_2O_2 detection by reacting with H_2O_2.[15] For example, Ye *et al.* reported novel fluorescent probes HKPerox-1 and HKPerox-2 based on the H_2O_2-responsive group and tandem Payne/Dakin reaction to molecular recognition of H_2O_2 (Fig. 2c).[54] A benzopyrylium-coumarin (BC) probe has been reported to detect H_2O_2.[55] And a fluorescent probe 7-hydroxy-2-oxo-*N*-(2-(diphenylphosphino)ethyl)-2*H*-chromene-3-carboxamide (DPPEA-HC) consisting of a 7-hydroxycoumarin moiety and a diphenylphosphine moiety have been designed to detect H_2O_2 (Fig. 2d).[56] Not only that, ABTS could be converted into oxidized ABTS in the presence of H_2O_2.[57] As depicted in Fig. 2e, oxidized ABTS possessed strong NIR absorbance, which could be used for PA imaging. Therefore, this implies that organic molecules-based nanomaterial may be an effective nanoplatform for H_2O_2-related diseases treatment and diagnosis.

2.1.2 Enzymes. There are amounts of enzymes that can react with H_2O_2, such as CAT, superoxide dismutase (SOD), horseradish peroxidase (HRP), peroxidase (POD) and so on.[58–60] For example, CAT, a H_2O_2-metabolizing enzyme, can catalyze H_2O_2 to generate O_2, which is an important pathway for H_2O_2 metabolism.[61,62] Then, the generation of O_2 can be used to alleviate hypoxia tumor microenvironment (TME) or convert to ROS. The involvement of CAT in tumor therapy is a major trend in biomedical fields. However, as a natural enzyme, it is easy to leak into the normal tissue before entering the tumor area, thus affecting the activity of normal cells. Similarly, its activity during the transportation is affected by the surrounding environment. To prevent organic molecules or enzymes' premature leakage and improve their delivery, nanocarriers were usually used to load them into disease regions. Organic carriers loading H_2O_2-related enzymes have the advantages, of high loading efficiency and good biocompatibility.[63] For instance, hyaluronic acid (HA) served as a biodegradable carrier to load CAT by covalent conjugation, which had tumor-targeting ability (Fig. 2f).[63] The encapsulated CAT could decompose endogenous H_2O_2 to produce oxygen and relieve hypoxia *in situ*. In other study, Chen *et al.* synthesized a core–shell nanoparticle-based poly(lactic-*co*-glycolic) acid (PLGA) to encapsulate CAT in order to protect CAT in Fig. 2g.[64]

2.1.3 Organic polymer nanoparticles. It is becoming increasingly apparent that organic polymer nanoparticles are widely used in H_2O_2-responsive biomedical fields because of their stability advantage.[65] For example, Park *et al.* synthesized polyoxalate containing vanillyl alcohol (PVAX) polymer nanoparticles for H_2O_2 scavenging and drug release.[66] Ou *et al.* designed prodrug-delivery nanoplatforms based on podophyllotoxin (POD) prodrug linking with poly(ethylene glycol)(*n*) monomethacrylate.[67] In the presence of H_2O_2, POD drugs could be released by a self-sacrificing pathway. In another study, Phan *et al.* reported the evolution of particle size and morphology of H_2O_2-sensitive block copolymer NPs from spherical micelles, fused micelles, to vesicles over time (Fig. 2h).[65] Not only that, polymers could also be used to detect H_2O_2.[68] Fluorescent single-chain polymer nanoparticles (SCNPs) with aggregation-induced emission (AIE) were used for H_2O_2 detection through intermolecular heavy-atom effect. Liu and coworkers designed a metalloporphyrin-based porous organic polymer which exhibited excellent peroxidase-like activity for detecting H_2O_2.[69] The polymer possessed a wide linear range of 50–1800 μM and a relative lower limit of detection (LOD) of 26.70 μM for H_2O_2.

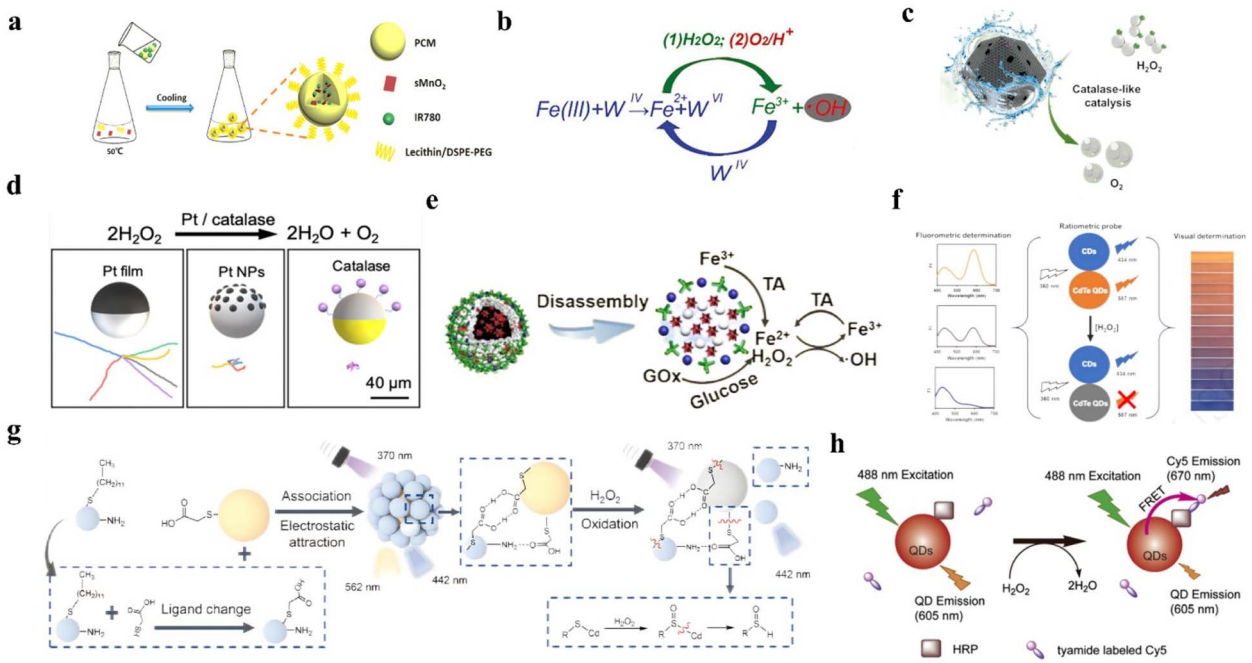

Fig. 3 (a) The synthetic process of IR780-sMnO$_2$-PCM NPs. Reproduced from ref. 82 copyright 2019, WILEY-VCH Verlag GmbH & Co. KGaA, Weinheim. (b) Schematic of Fe(III)@WS$_2$-PVP nanocapsules to generate Fe^{2+} and trigger a Fenton reaction. Reproduced from ref. 91 copyright 2018, American Chemical Society. (c) Schematic of The Fe-SAzyme exhibited CAT-like capacity to decompose H_2O_2 to O_2. Reproduced from ref. 96 copyright 2022, Wiley-VCH GmbH. (d) Schematic of Pt NPs catalyzed H_2O_2 and the synthetic process of Pt NPs. Reproduced from ref. 104 copyright 2021, American Chemical Society. (e) Schematic of TA reducing Fe(III) to Fe(II). Reproduced from ref. 113 copyright 2018, American Chemical Society. (f) The schematic of MPA-CdTe QDs to detect H_2O_2. Reproduced from ref. 115 copyright 2019, Elsevier B.V. (g) Schematic of Si–CdTe hybrid QDs to detect H_2O_2. Reproduced from ref. 116 copyright 2022, Wiley-VCH GmbH. (h) Schematic of QDs labeled Cy5 to detect H_2O_2. Reproduced from ref. 118 copyright 2012, Elsevier B.V.

Therefore, the polymer could accurately detect the change of H_2O_2 under physiological and pathological conditions.

2.1.4 Hydrogels. As a safe material, hydrogels have many advantages, such as high porosity, which is conducive to substance exchange and drug loading.[70] At the same time, hydrogels are sensitive to external stimuli, such as pH, redox, and so on.[71] Therefore, these advantages can be utilized to design hydrogels with H_2O_2-response for drug delivery or H_2O_2 detection. For example, Ren *et al.* designed a novel H_2O_2-responsive hydrogel based on the thiazolidinone group.[71] With the addition of H_2O_2, hydrogels underwent gel–sol phase transition, which was used for drug release (Fig. 2i). In other studies, hydrogels also had great applications in the field of biosensing.[72–74] Guo *et al.* designed L012@PAni-PAAm hydrogels as biosensors to monitor H_2O_2 produced from cardiomyocytes.[72]

In conclusion, organic nanomaterials play a very important role in H_2O_2-related biomedical applications. Reasonable design of organic nanomaterials with higher safety, better therapeutic efficiency and more functionality is the focus of future research.

2.2 H_2O_2-responsive inorganic nanomaterials

Owing to the advancement of nanotechnology, many inorganic materials now have possessed enzyme-mimic catalytic effects, mainly including oxidase-like, peroxidase-like, CAT-like, and superoxide dismutase-like.[75,76] Compared with natural enzymes, inorganic materials have amounts of advantages, such as facile fabrication, low cost, and robust stability against severe conditions.[77] In this part, we list four types of H_2O_2-responsive inorganic nanomaterials: metal oxides, metal ions, single-atom nanozymes, and noble metal nanoparticles.

2.2.1 Metal oxides. Currently, various metal oxide inorganic materials, which served as enzyme mimics have been reported that could directly or indirectly react with H_2O_2, such as manganese (Mn), cobalt (Co), cerium (Ce), and ruthenium (Ru).[78–80] For example, H_2O_2 would be catalyzed to O_2 by manganese dioxide (MnO_2).[81] Then, the increasing concentration of O_2 could be used to enhance the therapeutic effect of various oxygen-dependent therapeutic methods. As shown in Fig. 3a, Zhang *et al.* loaded MnO_2 and IR780 into a thermal-responsive phase-change material (IR780-sMnO$_2$-PCM NPs) for enhancing the photodynamic therapy effect.[82] In addition to Mn, Co-based metal oxides have been proven that possessed SOD-like, CAT-like, and POD-like catalytic activities.[83,84] Based on those, cobaltosic oxide (Co_3O_4) nanoparticles have been designed as biosensing platforms to detect H_2O_2.[85] In another study, Ce-based metal oxides have been reported that the ratio of Ce^{3+}/Ce^{4+} determined the enzyme-like properties, such as CAT mimic.[86] In addition, vanadium (V)-based and titanium (Ti)-based metal oxides exhibited POD-like activity that has been reported.[87,88]

2.2.2 Metal ions. As with metal oxides, metal ions can also react with H_2O_2, such as Mn ions (Mn^{2+}), Fe ions (Fe^{2+}), cuprum ions (Cu^{2+}), and so on.[89] The main mechanism of the reaction with H_2O_2 is Fenton or Fenton-like reaction. For example, Zhu *et al.* synthesized a nanoplatform that could release Mn^{2+} in the presence of overexpressed glutathione (GSH).[90] Subsequently, Mn^{2+} was oxidized by H_2O_2 and generated toxic $^{\bullet}OH$. Besides Mn ions, Fe(III)@WS_2-PVP nanocapsules to generate Fe^{2+} and trigger a Fenton reaction have been designed (Fig. 3b).[91] In the nanocapsule, the Fe(III) was reduced to form Fe^{2+} by WS_2. Then, the continuously generated Fe^{2+} reacted with H_2O_2 to produce $^{\bullet}OH$ in tumor cell. The same as irons, Cu^{2+} and Co^{2+} have been proven to trigger the H_2O_2 to generate $^{\bullet}OH$.[92,93]

2.2.3 Single-atom nanozymes. Recently, a single-atom enzyme (SAzyme) has been reported to apply for developing H_2O_2-related biomedicines due to its unique catalytic properties.[94] For example, SAzyme possesses POD-like activity which catalyzed H_2O_2 into $^{\bullet}OH$ in the TME.[95,96] Zhang *et al.* designed an Fe-based SAzyme by edge-site engineering, which exhibited CAT-like capacity to decompose H_2O_2 to O_2, and the edge-site engineering would enhance the CAT-like activity (Fig. 3c).[96] The Fe-SANzyme significantly removed ROS and reduced oxidative stress through CAT-like catalysis, thereby eliminating pathological angiogenesis in animal models of retinal angiopathies without affecting normal vascular repair. And a novel palladium (Pd)-based SAzyme, which could generate $^{\bullet}OH$ in the presence of H_2O_2 has been synthesized.[97] At present, the research on H_2O_2-related SAzymes is still in its infancy, and it will be a hot spot in future research.

2.2.4 Noble metal nanoparticles. Like metal oxides, some noble metal nanoparticles can produce or consume H_2O_2, such as aurum (Au), platinum (Pt), ruthenium, and palladium.[83,94,98–100] For example, Pt, a common noble metal, is often used to catalyze H_2O_2 due to its CAT-like ability, electrochemical production, *etc.*[101–103] As depicted in Fig. 3d, silicon dioxide (SiO_2)–Pt NPs have been designed, which could decompose H_2O_2 to O_2 as like CAT.[104] In other research, a motor that combined Au and Pt moved along a stable direction by the catalytic decomposition of H_2O_2.[105] And, Ru nanoparticles and Pd-based nanozymes have been proven that exhibited HRP, CAT, or POD-like activities.[100,106] Ye *et al.* reported Ru nanoframes with an octahedral shape that were three times more active than natural POD.[107] Furthermore, noble metal alloy nanoparticles, such as iridium (Ir)/Ru and Pt/Cu alloy nanoparticles, also exhibited enzyme-like activities.[108,109] Thus, the applications of noble metal in H_2O_2-responsive nanomaterials are showing great potential for the theranostic of diseases.

2.3 Hybrid nanomaterials

Most hybrid nanomaterials are composed of close integration of organic components, inorganic components, or dual types of ingredients.[110] Hybrid materials can combine the advantages of organic and inorganic materials for more efficient biological applications.

2.3.1 Metal–organic frameworks. Metal–organic frameworks (MOFs), a type of hybrid material, are consisted of metal ions (or clusters) and organic groups, and their role in nanomaterials is becoming central.[111] Recently, many researches have shown that MOF could serve as a nanozyme, which would react with H_2O_2.[112] For example, Cheng *et al.* reported a nanoplatform ICG@Mn/Cu/Zn-MOF@MnO_2 that could be used for synergistic tumor treatment.[24] The nanoplatform could release Cu^{+} and Mn^{2+} to catalyze H_2O_2 into $^{\bullet}OH$ in tumor cells. More than that, the organic components of MOF could assist inorganic components for H_2O_2-related applications. For instance, tannic acid (TA) could quickly reduce Fe(III) to Fe(II), and then Fe(II) catalyzed H_2O_2 to $^{\bullet}OH$ (Fig. 3e).[113]

2.3.2 Quantum dots and their capping agents or coating. Because of their unique optical properties, quantum dots (QDs) were widely used for fluorescence-based sensing.[114] H_2O_2-sensitive QDs have been designed to detect H_2O_2 *via* coating organic molecules.[114] Castro *et al.* designed a 3-mercaptopropionic acid (MPA) capped cadmium telluride (CdTe) QDs with orange-emitting and combined with a blue-emitting carbon dot (CD).[115] When H_2O_2 was not present, MPA-CdTe QDs and CDs could produce fluorescence signals of different wavelengths, respectively (Fig. 3f). With the addition of H_2O_2, the emitting fluorescence of MPA-CdTe QDs was decreased while the emitting fluorescence of CDs remained constant. The change of fluorescence signal was linearly correlated with H_2O_2. Using this special fluorescence signal change, it could be used as a method to determine H_2O_2. In another study, water-soluble Si–CdTe hybrid QDs have been designed to detect H_2O_2.[116] In the presence of H_2O_2, the fluorescence of CdTe QDs was extinguished due to the breakage of the Cd–S bond (Fig. 3g). Furthermore, Te-doped CDs have been reported to scavenge H_2O_2 for protecting normal cells.[117] In addition to fluorescence attenuation, QDs-related fluorescence enhancement could also be used to detect H_2O_2. For example, Huang *et al.* reported a new strategy of fluorescence resonance energy transfer (FRET) for enhanced fluorescence in the HRP-catalyzed oxidation with H_2O_2.[118] In the presence of H_2O_2, the QDs served as a fluorescent donor, and the tyramide labeled Cy5 served as an acceptor to generate a fluorescent wavelength of 670 nm (Fig. 3h).

2.3.3 Noble-metal nanoclusters and organic protective agents. Noble-metal nanoclusters can be served as biomedical probes to detect H_2O_2 due to their excellent fluorescence properties.[119] Chen *et al.* utilized bovine serum albumin (BSA) as a stabilizer to synthesize argentum nanoclusters (AgNCs), which could be applied for selectively H_2O_2 detection.[120] Wang *et al.* prepared a fluorescent probe AgNC which was collaboratively composed of pyridinium-based ionic liquid.[121] The original fluorescence could be quenched by the coordination bond between AsO_3^{3-} and π molecular orbitals. With the addition of H_2O_2, AsO_3^{3-} could be oxidized to AsO_4^{3-} and the origin fluorescence would recover. In addition to Ag, Au nanoclusters (HRP-AuNCs) have also been used to investigate H_2O_2 secretion at the single-cell level.[122] Not only that, organic agents-stabilized Cu nanoclusters have also served as H_2O_2-responsive fluorescent probes in biomedical applications.[123]

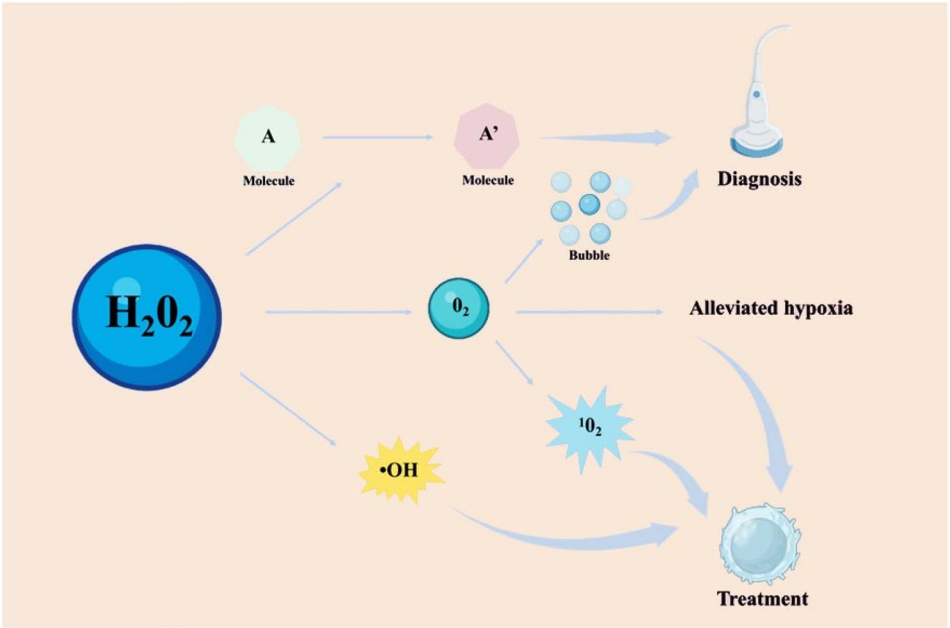

Fig. 4 The typical mechanism of H_2O_2-responsive nanomaterials in the biomedical applications.

To summarize, an increasing number of H_2O_2-responsive nanomaterials, such as organic, inorganic, and hybrid nanomaterials, are being employed in a variety of biological applications. Future research will also concentrate on the discovery novel nanomaterials as well as the advancement of existing nanomaterials. In the subsequent sections, we summarize and review the various biomedical applications of novel nanomaterials, including disease therapy and imaging.

3 The mechanism of H_2O_2-responsive nanomaterials for biomedical applications

The mechanism of H_2O_2 responsive nanomaterials can be broadly divided into three categories: (1) utilize H_2O_2 to change the state of organic molecules; (2) eliminate H_2O_2 and produce oxygen; (3) catalyze H_2O_2 to produce hydroxyl radical. For the former (1), the H_2O_2 can directly affect the nanomaterials composed of ABTS molecules, aromatic boronates-based molecules, or fluorescent molecules, causing the change of their characteristic absorption or emission peak, or the cleavage of molecules. For the latter (2) and (3), the by-products such as O_2, $^{\bullet}OH$, and metal ions, generated by those nanomaterials and H_2O_2 reactions played central role in their biological applications. For example, the generation of $^{\bullet}OH$ by catalyzing H_2O_2 can cause oxidative stress, which can then induce tumor cells or bacterial death. The generation of O_2 by decomposed H_2O_2 can alleviate hypoxia, or be converted into $^1O_2$, or be used as US contrast agents for enhancing the effect of disease treatment. Another example, a lot of ions can react with H_2O_2 through a Fenton reaction or a Fenton-like reaction and can be monitored by magnetic resonance imaging. Here, we listed the main usage mechanisms of H_2O_2 (Fig. 4).

4 Biomedical applications of H_2O_2-responsive nanomaterials

The occurrence and progression of many diseases are closely related to H_2O_2 levels. Reasonable selection of H_2O_2 treatment methods is of great help into the treatment and diagnosis of diseases. H_2O_2-related diseases treatment mainly relies on oxidative stress from H_2O_2 generated ROS, increasing oxygen content for various therapy methods and removing H_2O_2. Thus, the H_2O_2-responsive nanomaterials are categorized into two different groups: (1) producing ROS and (2) reducing oxidative stress. The former included tumors, bacterium, dental diseases. The latter included inflammations, cardiovascular diseases, bones, neurologic diseases and ophthalmic diseases. H_2O_2-related imaging diagnosis are based on the release product of nanomaterials after interacting with H_2O_2, such as gas bubbles, metal ions, and fluorescence signal changes. Herein, we provide an overview of current researches on H_2O_2-related various therapy and imaging detection applications (Table 2).

4.1 Enhanced tumor therapy effect by producing ROS and correlated imaging

As a major threat to human health, it has always been the goal of tumor nanomedicine to develop effective treatments.[125] In this section, we will provide an overview of current researches on H_2O_2-involving tumor therapy and diagnosis.

4.1.1 Enhanced tumor therapy by enhancing $^1O_2$ production and alleviating hypoxia. Photodynamic therapy (PDT), sonodynamic therapy (SDT), radiotherapy (RT), radiodynamic therapy (RDT) and immunotherapy have emerged as novel tumor treatment strategies as a result of the advancement of nanotechnology.[64,126–129] The main mechanism of PDT, SDT, and RDT is the transfer of electrons or energies from sensitizers to

Table 2 Categorization of H_2O_2-responsive nanomaterials in recent years

Research field	Method	Nanomaterial	Mechanism	Application	Ref.
Tumors	Treatment	Mn-CDs	Produce O_2	Enhanced PDT	Jia *et al.*[7]
		Ce6-DNAzyme NPs	Convert H_2O_2 to $^{\bullet}OH$ for type I PDT	Combined type I and II PDT	Liu *et al.*[27]
		CSI@Ex-A	Produce O_2 *via* CAT	Enhanced SDT	Wu *et al.*[138]
		HMONs-MnOx	Produce O_2 *via* Mn-based nanozymes	Enhanced SDT	Zhu *et al.*[140]
		GDY–CeO_2–miR181a–PEG–iRGD	Produce O_2 *via* CeO_2	Enhanced RT	Zhou *et al.*[143]
		AVPt@HP@M	Produce O_2 *via* Pt NPs	Enhanced RT	Gong *et al.*[141]
		PLGA-R837@CAT	Produce O_2 *via* CAT	Enhanced immunotherapy	Chen *et al.*[64]
		AFe NPs	Generate $^{\bullet}OH$ *via* Fe^{2+}	Enhanced CDT	Chen *et al.*[158]
	Imaging	MS@MnO_2 NPs	Deplete GSH and produce $^{\bullet}OH$	Enhanced CDT	Lin *et al.*[159]
		Cu_2MoS_4@GOx	Enhance multiple enzyme effect	Synergistic therapy	Chang *et al.*[21]
		ACD	Turn on the fluorescence	H_2O_2-responsive FLI	Zhao *et al.*[171]
		Ag/Ag_2S NPs	Turn on the fluorescence	FLI of liver injury and tumor	Zhang *et al.*[172]
		GQDzyme/ABTS NPs	Convert ABTS into oxidized ABTS	PAI of nasopharyngeal carcinoma *in vivo*	Ding *et al.*[57]
		LOD/CAT-loaded nanogels	Generate abundant O_2 gas	Efficient diagnostic nanoprobes of US imaging	Wu *et al.*[180]
		AuNCs@mSiO_2@MnO_2	Release Mn^{2+}	Enhanced MRI signal intensity	Yin *et al.*[185]
		MnPcE4	Achieve trimodal imaging	Achieved multimodal imaging	Wang *et al.*[187]
Bacterium	Treatment and imaging	CoIITBPP(bpy) nanozymes	Enhance CAT-like activity	Enhanced PDT	Hu *et al.*[8]
		Pd@Pt-T790 NPs	Produce O_2 *via* Pt NPs	Enhanced PDT and combined PAI and MRI	Sun *et al.*[191]
		Cu_2O NPs	Catalyze H_2O_2 to $^{\bullet}OH$	Combined CDT and PAI	Yang *et al.*[193]
		Ce6@Arg-ADP NPs	Produce NO *via* H_2O_2	NO therapy	Zhu *et al.*[33]
Dental diseases	Treatment and imaging	TiO_2/Pt tubular robots	Generate bubbles and $^{\bullet}OH$	Oral biofilm disruption	Villa *et al.*[196]
		Dex-IONP-GOx NPs	Generate $^{\bullet}OH$	Prevent dental caries	Huang *et al.*[13]
		CuO/BP nanosheets	Conversion from H_2O_2 to O_2 is related valence change of Cu	Assessment of disease progression and treatment effectiveness	Wang *et al.*[197]
Inflammations	Treatment	2D-TMD nanosheets	Scavenge intracellular H_2O_2	Anti-inflammation	Yim *et al.*[32]
		Hollow microspheres	Release drugs and CO_2 gas by H_2O_2	Anti-inflammation	Chung *et al.*[200]
	Imaging	TMSN@PM	Reaction with H_2O_2 and degrades itself to release Mn^{2+}	Switch of MRI signal	Li *et al.*[203]
		Au–Pd@Ag nanorods	Variate absorption *via* H_2O_2	Therapeutic effect evaluation by PAI	Ye *et al.*[34]
		CUR-PVAX NPs	Degrade peroxalate ester to generate CO_2 bubbles	Potential US agents of ischemic diseases	Jung *et al.*[204]
		Co complexes	Utilizing the large change in chemical shift shown at 19F	Therapeutic effect evaluation by MRI	Yu *et al.*[205]
Cardiovascular diseases	Treatment	Hydrogels contained CAT	Scavenge H_2O_2	MI repair	Ding *et al.*[209]
		nCe-decorated nanofibers	Scavenge H_2O_2	Cardiac hypertrophy inhibition	Jain *et al.*[210]
		Fu-sBR nanoassemblies	Scavenge H_2O_2	Thrombosis treatment	Jung *et al.*[211]

Table 2 (*Contd.*)

Research field	Method	Nanomaterial	Mechanism	Application	Ref.
	Imaging	BSA-Cy-Mito nanoprobes	Produce PAI signal	Atherosclerotic plaque vulnerability assessment and precise treatment	Gao *et al.*[212]
Bone injury	Treatment and imaging	Pt/CeO_2 nanozymes	Multiple enzyme effects scavenge uric acid and H_2O_2	Treatment of MSU-induced acute gout	Lin *et al.*[230]
		PUDCA NPs	Scavenge H_2O_2 and release UDCA	The osteogenic differentiation of MSCs	Arai *et al.*[5]
		Fe_3O_4@GO/BMP2	Reduce H_2O_2 and capture $^{\bullet}OH$	Bone tissue regeneration	Zhang *et al.*[232]
		hMNP/GelMA composite hydrogels	Scavenge H_2O_2 and release Mn^{2+} for promoting osteogenesis	Bone tissue regeneration	Li *et al.*[234]
Neurologic diseases	Treatment	Ma@(MnO_2 + FTY) NPs	Convert H_2O_2 to O_2	Protect damaged neurons	Li *et al.*[238]
	Imaging	PCAB	Detect H_2O_2	Therapeutic effect evaluation by FLI	Wang *et al.*[240]
		CRANAD-88	Amplifying NIR fluorescence signals	Monitoring the changes of H_2O_2 concentrations before and after treatment	Yang *et al.*[241]
Ophthalmic diseases	Treatment	CeNP-CL	Scavenge H_2O_2	Treatment of ophthalmic diseases	Choi *et al.*[245]

adjacent substrates, under light, US, or X-ray irradiation, followed by the production of ROS.[9] While the main mechanism of enhanced RT and immunotherapy is changing the microenvironment of RT and the immune by alleviating hypoxia. The concentration of O_2 plays a key role in those therapies, which are positively correlated with the therapeutic effect. However, due to the rapid proliferation of tumor cells and insufficient blood supply, hypoxia becomes an important characteristic of

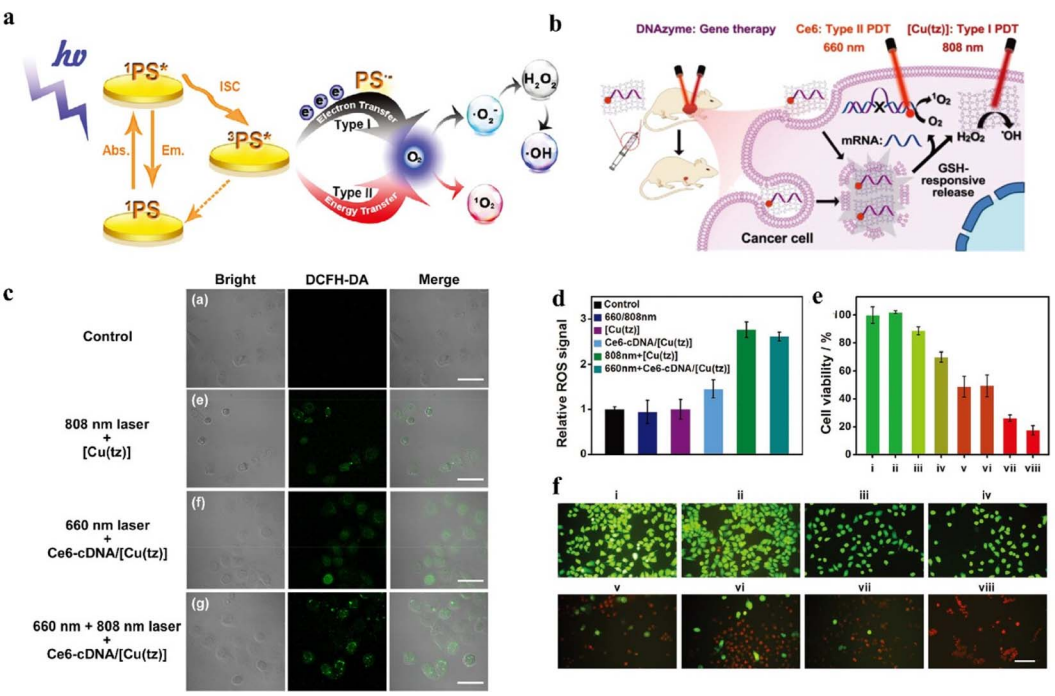

Fig. 5 (a) Schematic of the difference between type I and type II. Reproduced from ref. 135 copyright 2021, Wiley-VCH GmbH. (b) Schematic of the nanoplatform to convert H_2O_2 to $^{\bullet}OH$ for tumor treatment. Reproduced from ref. 27 copyright 2021, Wiley-VCH GmbH. (c) Confocal images of intracellular ROS generation. Reproduced from ref. 27 copyright 2021, Wiley-VCH GmbH. (d) ROS fluorescence signals generated during different treatments. Reproduced from ref. 27 copyright 2021, Wiley-VCH GmbH. (e) Cell viability of MCF-7 cells with different treatments. Reproduced from ref. 27 copyright 2021, Wiley-VCH GmbH. (f) Live/dead staining images of MCF-7 cells with different treatments. Reproduced from ref. 27 copyright 2021, Wiley-VCH GmbH. PBS (i), 660 and 808 nm laser irradiation (ii), Ce6-cDNA/[Cu(tz)] (iii), Ce6-DNAzyme/[Cu(tz)] (iv), Ce6-cDNA/[Cu(tz)] under 660 nm laser irradiation (v), [Cu(tz)] under 808 nm laser irradiation (vi), Ce6-DNAzyme/[Cu(tz)] under 660 nm laser irradiation (vii), and Ce6-DNAzyme/[Cu(tz)] under 660 and 808 nm laser irradiation (viii).

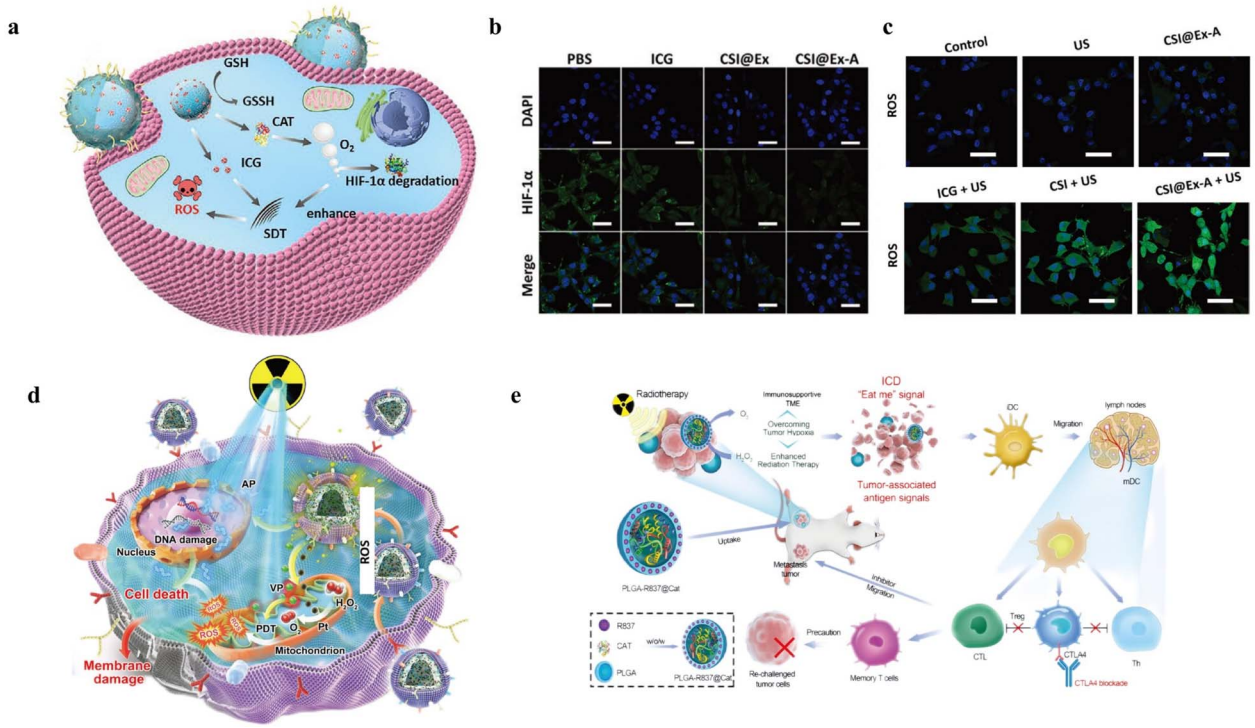

Fig. 6 (a) Schematic illustration of CSI@Ex-A nanoplatforms based on CAT and ICG for SDT. Reproduced from ref. 138 copyright 2022, Wiley-VCH GmbH. (b) HIF-1α fluorescence signals generated during different treatments. Reproduced from ref. 138 copyright 2022, Wiley-VCH GmbH. (c) ROS fluorescence signals generated during different treatments. Reproduced from ref. 138 copyright 2022, Wiley-VCH GmbH. (d) Schematic illustration of the synthetic process of Pt and apoptin-based nanoplatform and its mechanism of alleviating hypoxia and enhancing RT. Reproduced from ref. 141 copyright 2022, Wiley-VCH GmbH. (e) Schematic of PLGA-R837@CAT NPs to trigger ICD and anti-CTLA4 checkpoint blockade. Reproduced from ref. 64 copyright 2019, WILEY-VCH Verlag GmbH & Co. KGaA, Weinheim.

tumors.[130] If the oxygen tension falls below 10 mmHg, tissue is generally classified as hypoxic.[131] Hypoxia-inducing factor 1 (HIF-1) is considered to be the main regulatory factor for cell adaptation to hypoxia, which is closely related to tumor progression and therapeutic effect.[132] It can make cells and tissues produce a series of reactions to adapt to hypoxia environment, promote tumor angiogenesis, and increase the tumor's own invasiveness and resistance to treatments.[4,26,29,133] Strategies for O_2 generation have been reported include exogenous delivery of O_2 to tumor region, or inhibition of mitochondrial respiration in tumor cells.[9] However, these methods all encountered the problem of insufficient oxygen loading effect.[9] At present, the decomposition of overexpressed H_2O_2 into O_2 by nanomaterials become an important method to alleviate hypoxia.[9]

4.1.1.1 Enhanced photodynamic therapy. PDT mainly uses photosensitizer to generate energy level transition under the excitation of light and enter the excited state of higher energy level.[134] Then, as the photosensitizer returns to its ground state, it needs to release a charge or energy to its surroundings. The substrate molecules around the photosensitizer gain this charge or energy to form ROS. PDT are divided into type I and type II by obtaining differences in charge or energy. PDT could be divided into type II (enhancing treatment by H_2O_2) and type I (direct treatment with H_2O_2) as shown in Fig. 5a.[135] The mechanism of type II was that converted O_2 from the decomposition of H_2O_2 into $^1O_2$. For instance, Jia and coworkers synthesized a nanoplatform (Mn-CDs) to enhance PDT.[7] Mn-CDs served as a CAT-like nanozyme to produce O_2 by H_2O_2, then as a photosensitizer to convert O_2 to $^1O_2$. The amount of $^1O_2$ produced was closely correlated with the concentration of O_2. The mechanism of type I was that the excited photosensitizer under light irradiation could react with adjacent substrates by electron transfer to produce ROS.[136] A GSH-responsive-release nanoplatform for H_2O_2-related type I PDT under 808 nm laser irradiation have been designed (Fig. 5b).[27] The nanosheet could not only convert H_2O_2 to $^{\bullet}OH$ under 808 nm laser irradiation for type I PDT, but also convert O_2 to $^1O_2$ under 660 nm laser irradiation for type II PDT. As shown in Fig. 5c and d, through DCFH-DA fluorescence in cells it was not difficult to find that the nanomaterial could produce ROS through type I and type II PDT under laser irradiation of different wavelengths. Moreover, cell viability in Fig. 5e and live/dead staining imaging in Fig. 5f showed that the killing ability of this nanomaterial against MCF-7 cells.

4.1.1.2 Enhanced sonodynamic therapy. SDT was also an excellent method of tumor therapies, which could generate ROS and possess maximum tissue-penetration depth.[28,137] Thus, the increasing concentration of O_2 could also enhance the effect of SDT. Inspired by the fact that H_2O_2 produced oxygen by CAT, Wu *et al.* designed a nanoplatform CSI@Ex-A for enhancing SDT (Fig. 6a).[138] The generated O_2 from the decomposition of H_2O_2 by CAT would be converted to $^1O_2$ by indocyanine green

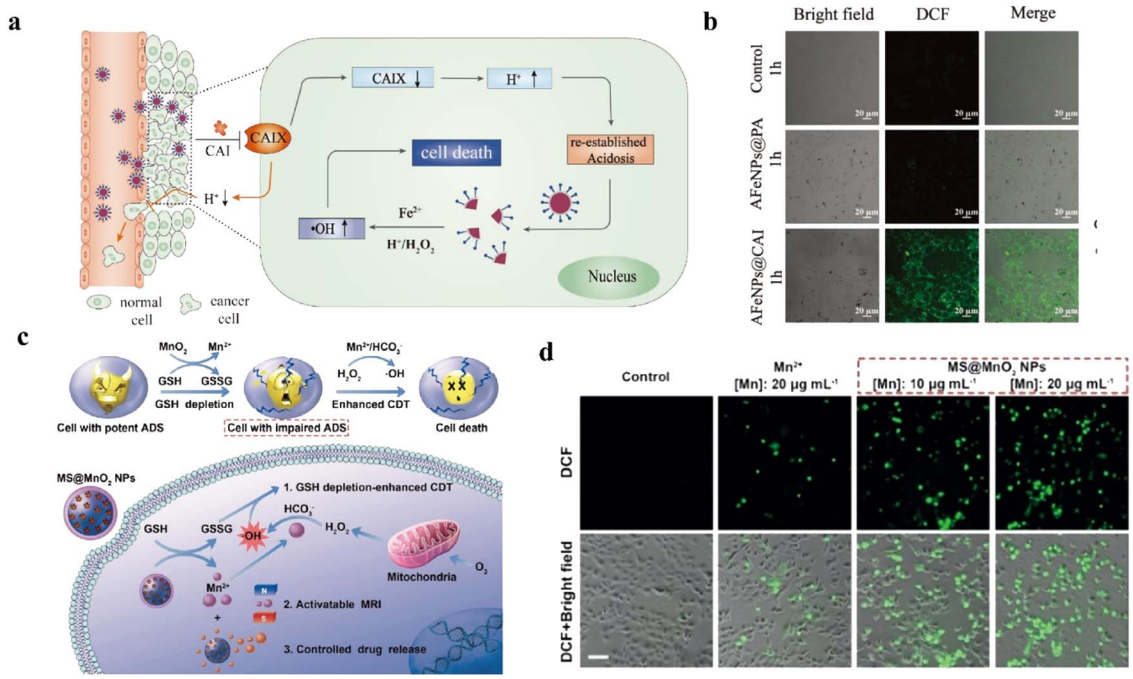

Fig. 7 (a) Schematic illustration of AFe NPs for self-enhanced CDT. Reproduced from ref. 158 copyright 2019, WILEY-VCH Verlag GmbH & Co. KGaA, Weinheim. (b) The fluorescence images of DCFH-DA with different treatments. Reproduced from ref. 158 copyright 2019, WILEY-VCH Verlag GmbH & Co. KGaA, Weinheim. (c) Schematic illustration of MS@MnO_2 NPs to deplete GSH and produce $^{\bullet}OH$ for CDT. Reproduced from ref. 159 copyright 2018, WILEY-VCH Verlag GmbH & Co. KGaA, Weinheim. (d) The fluorescence images of DCFH-DA with different treatments. Reproduced from ref. 159 copyright 2018, WILEY-VCH Verlag GmbH & Co. KGaA, Weinheim.

(ICG) under US irradiation. According to the HIF-1α fluorescence pattern analysis in Fig. 6b, it could be seen that CAT decomposed H_2O_2 to produce O_2, which could degrade HIF-1a to enhance the efficacy of tumor therapy. As shown in Fig. 6c, the DCFH-DA fluorescence image showed that the nanomaterial had the ability of SDT to produce ROS, and CAT could enhance the SDT effect. Meanwhile, the use of ultrasonic excitation compensated for the lack of penetration of light. In addition to CAT, Mn-based nanomaterials could also serve as a H_2O_2-responsive nanozyme for SDT.[139] For example, Zhu *et al.* designed a protoporphyrin-based nanoplatform that loaded into the hollow mesoporous organosilica nanoparticles (HMONs)-MnO_x to generate O_2 for enhancing SDT.[140]

4.1.1.3 Enhanced radiotherapy and radiodynamic therapy. After X-ray irradiation, oxygen molecules can inhibit DNA repair and HIF-1 expression enhancing the effect of Radiotherapy.[129] Hypoxia can mitigate DNA damage as well as reduce the absorption of radiation, which makes the resistance of the tumor to RT.[142] Hence, the rational design of nanomaterials for relieving hypoxia and enhancing tumor RT has been a hot area of research for several years. Zhou *et al.* reported a high-Z CeO_2-based nanoplatform for decomposing H_2O_2 to O_2 and enhancing RT.[143] The nanoplatform exhibited CAT-mimic activity, induced DNA damage and inhibited tumor growth. Similar nanoplatforms based on Pt NPs as CAT-like nanozymes have been designed for enhancing RT (Fig. 6d).[141] This nanoplatform possessed pH-responsive property, worked as radiosensitizer and had CAT-like activity to improve radiotherapy sensitivity. Compared with no oxygen supply, this strategy highly enhanced the effect of RT. Not only that, Sun *et al.* presented the RDT mechanism based on the X-ray excitation that transformed O_2 to $^1O_2$, combining the advantages of RT and PDT.[144]

4.1.1.4 Enhanced immunotherapy. For immunotherapy of cancer, alleviated hypoxia environment can also be used to enhance their effect.[145] Some studies have been reported that the therapy effect could be weakened by hypoxic-mediated immune suppression.[146] Therefore, alleviating hypoxia to enhance immunotherapy is a feasible tumor treatment strategy. Chen *et al.* designed poly PLGA-R837@CAT nanoparticles to produce O_2 for increasing immunogenic cell death (ICD) and then combined with anti-cytotoxic T-lymphocyte-associated antigen 4 (CTLA4) checkpoint blockade (Fig. 6e).[64] This nanoparticle was based on the core–shell PLGA nanoparticle to load CAT for synergistic oncotherapy. The PLGA-R837@CAT nanoparticle could destruct primary cancers under X-ray radiation and trigger the immunogenic cell death. This study was mainly based on oxygen relieving immunosuppressive tumor microenvironment. Moreover, hypoxia has been reported to facilitate immune-supportive M1-type tumor-associated macrophages (TAM) to immune-suppressive M2-type TAM, which was a disadvantage for immunotherapy.[147] Therefore, the production of O_2 by decomposed H_2O_2 had also attracted tremendous attention for immunotherapy.

4.1.2 Enhanced tumor therapy by $^{\bullet}OH$ production. In addition to producing oxygen, H_2O_2 can be used to produce $^{\bullet}OH$

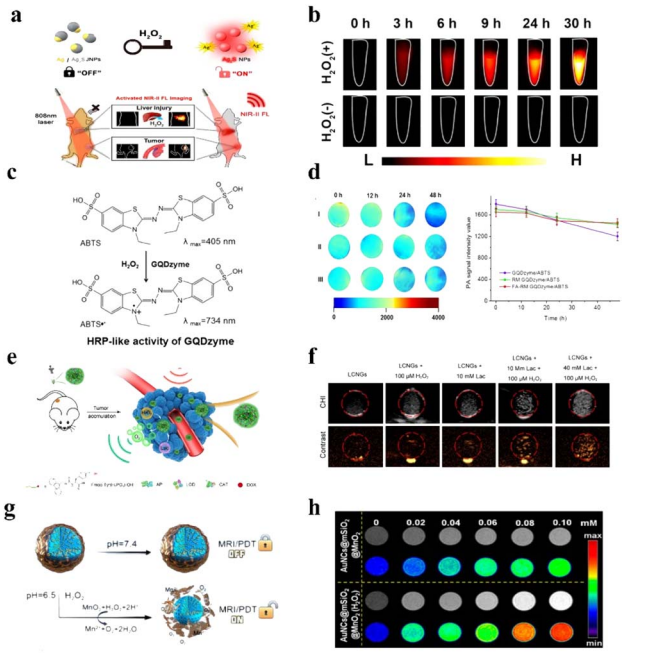

Fig. 8 (a) Schematic of Ag/Ag_2S Janus NPs for H_2O_2-activated NIR-fluorescence imaging. Reproduced from ref. 172 copyright 2021, American Chemical Society. (b) The change of fluorescence intensity under different conditions. Reproduced from ref. 172 copyright 2021, American Chemical Society. (c) Schematic illustration of ABTS for photoacoustic imaging. Reproduced from ref. 57 copyright 2019, American Chemical Society. (d) The change of PAI signal intensity. Reproduced from ref. 57 copyright 2019, American Chemical Society. (e) Schematic of nanoplatforms to continuously release oxygen bubbles for US imaging. Reproduced from ref. 180 copyright 2021, American Chemical Society. (f) The change of US intensity of in the tumor region. Reproduced from ref. 180 copyright 2021, American Chemical Society. (g) Schematic of AuNCs@mSiO_2@MnO_2 nanozymes for MRI. Reproduced from ref. 185 copyright 2021, American Chemical Society. (h) The change of MRI intensity of AuNCs@mSiO_2@MnO_2 nanozymes. Reproduced from ref. 185 copyright 2021, American Chemical Society.

for tumor treatment. Chemodynamic therapy (CDT) is an emerging, minimally invasive, and effective cancer treatment, which is based on the H_2O_2 induce $^{\cdot}OH$ formation *via* the Fenton or Fenton-like reaction.[10,148] Hydroxyl radical possesses efficient oxidative stress capacity for killing tumor cells.[149,150] Many nanomaterials have been reported that could be used for CDT, such as Fe-based, Mn-based, and other-based materials.[151–156] Fe-based materials have been widely used in the biological field because of their high biosafety.[148] The production of $^{\cdot}OH$ could be induced by the reaction between Fe^{2+} and H_2O_2 in acidic environments.[157] Then, the $^{\cdot}OH$ as a type of ROS could cause lipid peroxidation (LPO).[10] Chen *et al.* designed unique amorphous iron nanoparticles (AFe NPs) which loaded with carbonic anhydrase IX inhibitor (CAI) for self-enhanced CDT based on the Fenton reaction (Fig. 7a).[158] The CAI could inhibit the expression of carbonic anhydrase IX, caused acidic ions to accumulate in the cell. The accumulated acidic ions could lower pH in cells and had an enhanced effect on CDT (Fig. 7b). Meanwhile, researchers found that Mn^{2+} and Cu^{2+} also have Fenton-like reaction.[92] Inspired by this, Lin *et al.* synthesized MnO_2-coated mesoporous silica (MS) NPs to deplete GSH and produce $^{\cdot}OH$ for CDT.[159] As depicted in Fig. 7c, the MnO_2 layer would release Mn^{2+}, then the production of Mn^{2+} could react with H_2O_2 to generate $^{\cdot}OH$. As shown in Fig. 7d, the DCF fluorescence in tumor cells by MS@MnO_2 NPs was higher than $MnCl_2$ at the same Mn concentration. This proved that MS@MnO_2 NPs could produce stronger oxidative stress effects in the process of CDT. Hence, Fenton or Fenton-like reaction-based CDT has shown the great potential for cancer treatment.

In addition, H_2O_2-related synergistic therapy based on glucose oxidase (GOx) or GOx-like nanomaterials that exhibited excellent properties, which often combined with other treatment methods for enhancing tumor therapy effect.[160] Chang *et al.* have designed a nanoplatform Cu_2MoS_4 for synergistic starvation therapy and CDT.[21] Starvation treatment can continue to produce H_2O_2 to replace the H_2O_2 consumed by CDT. In other studies, H_2O_2-related gas therapy has also been reported.[161] Therefore, H_2O_2-related therapy strategies play important roles in the research of tumor therapy.

4.1.3 Enhanced tumor therapy by H_2O_2-related imaging guidance. Currently, H_2O_2-related tumor imaging methods commonly used mainly include fluorescence imaging (FLI), magnetic resonance imaging (MRI), ultrasound imaging (USI), photoacoustic imaging (PAI), *etc.* Each of imaging strategies has its own advantage. For example, FLI is an emerging tumor molecular imaging method, which possesses the advantages of high spatial and temporal resolution.[162] Overexpression of H_2O_2, a characteristic of TME, is widely believed to be involved in regulating the proliferation and malignant characteristics of cancer cells.[3] Therefore, qualitative and quantitative research on H_2O_2 is conducive to understanding the progression of tumor development and judging the effect of related treatment. For instance, Yu *et al.* designed a lapachone-loaded H_2O_2-responsive nanoplatform to detect tumor by the H_2O_2-related chemiluminescence.[163]

4.1.3.1 H_2O_2-related fluorescence imaging of tumor. In the field of biosensing, FLI can be used to detect the disorder of H_2O_2 in tumor.[164–170] The mechanism of H_2O_2-related FLI is mainly based on the fluorescence signal changes with the concentration of H_2O_2. For instance, Zhao *et al.* synthesized Cu ion-doped zeolitic imidazolate framework-8 (ZIF-8) loaded with AuNCs and DOX for FL imaging-guided therapy.[171] When the pH decreased and H_2O_2 existed, DOX and Cu ions would be released, then fluorescence signals of DOX and AuNCs could be recovered. In other studies, a Janus nanoparticle Ag/Ag_2S Janus NP has been designed for the diagnosis of disease and detection of H_2O_2 by H_2O_2-activated NIR-fluorescence imaging.[172] Due to the plasmonic electron transfer, the Janus NP possessed the ability of fluorescence quenching. The H_2O_2 served as a key to turn on the fluorescence signals under NIR irradiation in Fig. 8a. As shown in Fig. 8b, compared with the group without H_2O_2, the group with H_2O_2 showed strong fluorescence signals. Meanwhile, the fluorescence intensity increased with the increase of the contact time between nanomaterials and H_2O_2. Undoubtedly, the further exploration of FLI in biomedical

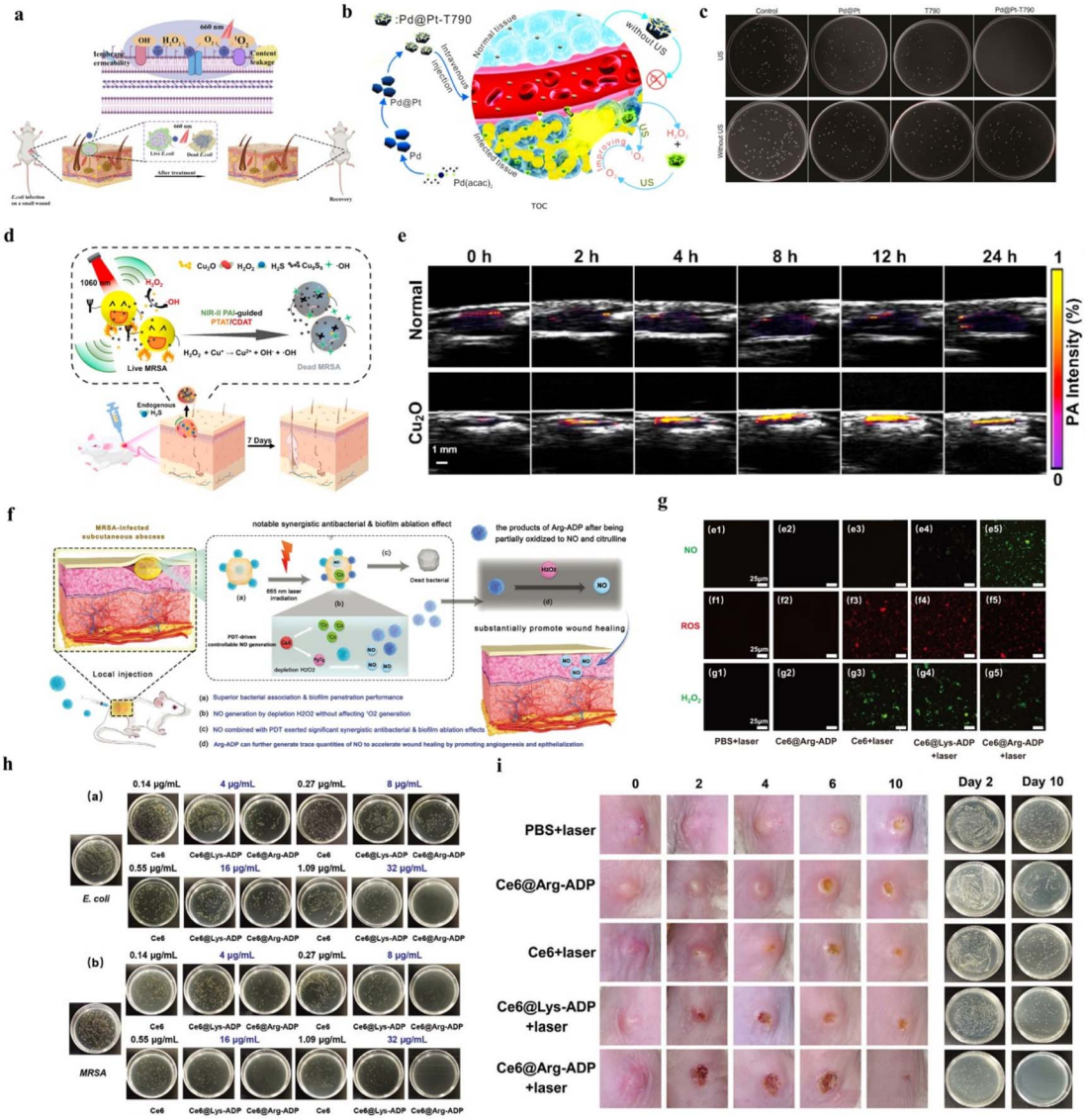

Fig. 9 (a) Schematic illustration of a phenylboronic acid-based nanozyme for synergistic antibacterial therapy. Reproduced from ref. 8 copyright 2021, Elsevier B.V. (b) Schematic illustration of a Pd@Pt-T790 nanotherapeutic platform for SDT. Reproduced from ref. 191 copyright 2020, American Chemical Society. (c) MRSA colony pictures after different treatments. Reproduced from ref. 191 copyright 2020, American Chemical Society. (d) Schematic illustration of Cu_2O nanoparticles for PA imaging-guided therapy. Reproduced from ref. 193 copyright 2021, Elsevier Ltd. (e) The PAI images of Cu_2O NPs *in vivo* at different time. Reproduced from ref. 193 copyright 2021, Elsevier Ltd. (f) Schematic illustration of Ce6@Arg-ADP for antibacterial therapy. Reproduced from ref. 33 copyright 2021, Wiley-VCH GmbH. (g) CLSM images of NO, ROS, and H_2O_2 generation in MRSA after different treatments. Reproduced from ref. 33 copyright 2021, Wiley-VCH GmbH. (h) Representative images of plate samples of *E. coli* and MRSA after different treatments. Reproduced from ref. 33 copyright 2021, Wiley-VCH GmbH. (i) Wound healing and colony change *in vivo*. Reproduced from ref. 33 copyright 2021, Wiley-VCH GmbH.

applications will be readily pushed forward by these new probes for H_2O_2.

4.1.3.2 H_2O_2-related photoacoustic imaging of tumor. Photoacoustic imaging (PAI) is also a promising diagnostic strategy that combines the advantages of traditional optical imaging and ultrasound imaging.[173] Briefly, a material undergoes thermoelastic expansion that is based on photothermal conversion under light irradiation, which is then converted to a US wave.[174] Some H_2O_2-responsive sensitizers possessed excellent properties for PA imaging, such as ABTS.[42] Ding *et al.* designed a nanoplatform to load ABTS for PAI, which was based on the strong NIR absorbance of ABTS.[57] The mechanism was based on the HRP-catalyzed colorless ABTS substrate into its green oxidized form in the presence of H_2O_2 (Fig. 8c and d). According to the change of PA signals, the fluctuation in H_2O_2 concentration could be analyzed. Hence, PA imaging can also become an important method for disease diagnosis and H_2O_2 detection in the biomedical application.

4.1.3.3 H_2O_2-related ultrasound imaging of tumor. Ultrasound imaging is an important tool in biomedical imaging fields due to its high resolution, non-invasive method, and real-time modality.[175,176] Recently, many researches have reported to

focus on contrast agents based on nanomaterials to produce gas bubbles in the tumor regions.[177,178] The generating bubbles could effectively reflect ultrasound signals, which were used for USI.[179] Wu *et al.* designed a nanosystem, which incorporated CAT and lactate oxidase (LOX), for enhancing US signals.[180] As shown in Fig. 8e, this nanoplatform could continuously release oxygen bubbles for USI by cascade catalysis of LOX and CAT. The continuously releasing oxygen bubbles could accumulate in the tumor region, which enhanced the specificity and continuity of USI (Fig. 8f). Thus, the generation of O_2 and the alleviation of hypoxia could be monitored. Besides, owing to its strong acoustic impedance, H_2O_2-induced CO bubbles could also serve as a contrast agent for USI.[181]

4.1.3.4 H_2O_2-related magnetic resonance imaging of tumor. Magnetic resonance imaging, a commonly used diagnostic tool, has the characteristics of high resolution, security, signal-to-noise ratio, and so on.[182] MnO_2 has been found that it could decompose H_2O_2 into water and oxygen, and release Mn^{2+} ions by itself.[183] The non-lanthanide metal ion Mn^{2+} could short the longitudinal relaxation time (T_1) and transverse relaxation time (T_2) of water protons, thus enhancing T_1-magnetic resonance imaging contrast and weakening T_2-magnetic resonance imaging contrast.[184] As shown in Fig. 8g, Yin and coworkers used this feature to design a H_2O_2-responsive nanozyme ($AuNCs@mSiO_2@MnO_2$) for enhancing MR signals.[185] Herein, according to the change of MR signals, the concentration of H_2O_2 could be analyzed in Fig. 8h.

4.1.3.5 H_2O_2-related multimodal imaging of tumor. H_2O_2-related multimodal imaging can combine the advantages of different imaging modalities.[186] For instance, Wang *et al.* designed a new type of phthalocyanine manganese (MnPcE4) photosensitizer to achieve trimodal imaging (*in vivo* FL/CT/MRI).[187] Fluorescence imaging showed that the nanomaterial was able to rapidly accumulate in the tumor area. Furthermore, in the presence of H_2O_2, the Mn^{2+} could release as well as be used for MR imaging. The complementary advantages of different imaging models greatly improved the application of H_2O_2-related imaging.

4.2 Bacterial infections therapy by producing ROS and correlated imaging

It has been demonstrated that H_2O_2 is also overexpressed in the microenvironment of bacterial infection regions.[8] Infections and unsuccessful wound healing caused by bacteria are among the serious health problems.[188] Utilizing H_2O_2 for producing ROS is an excellent antibacterial therapy.[31] This is because ROS destroy the bacterial membrane and damaged DNA, leading to bacterial death.[189]

As with tumor treatment, H_2O_2-related antibacterial therapy mainly includes PDT, SDT, and CDT.[190–192] As described in Fig. 9a, Hu *et al.* designed a phenylboronic acid-based nanozyme for antibacterial PDT.[8] Sun *et al.* synthesized a Pd@Pt-T790 therapeutic nanoplatform with organic sonosensitizer meso-tetra(4-carboxyphenyl)porphine (T790) for bacterial therapy (Fig. 9b).[191] The nanoplatform catalyzed H_2O_2 to produce O_2 and converted it into ROS under US irradiation. As shown in Fig. 9c, the results of colony counting showed that Pd@Pt-T790 nanoplatforms had good antibacterial effect of

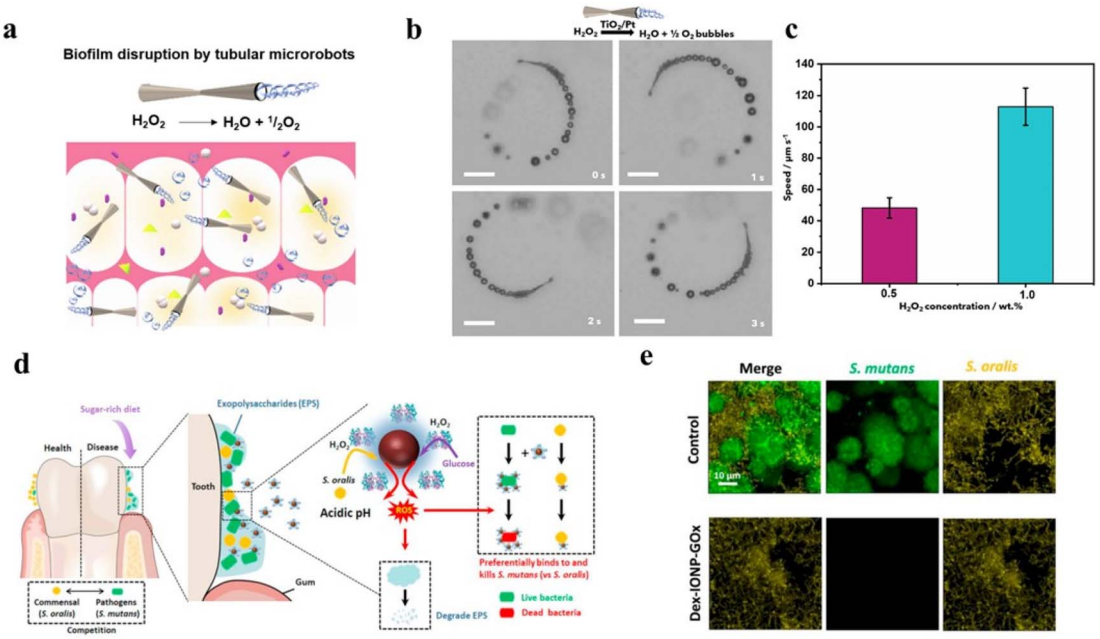

Fig. 10 (a) Schematic illustration of self-propelled tubular microrobots to disrupt biofilms. Reproduced from ref. 196 copyright 2020, Elsevier. (b) Snapshot images of TiO_2/Pt microrobots moving in different solution. Reproduced from ref. 196 copyright 2020, Elsevier. (c) Speed of the TiO_2/Pt microrobots at different concentrations of H_2O_2. Reproduced from ref. 196 copyright 2020, Elsevier. (d) Schematic illustration of Dex-IONP-GOx nanoplatforms for prevention of dental caries. Reproduced from ref. 13 copyright 2021, Elsevier Ltd. (e) Fluorescence images of survival of different bacteria. Reproduced from ref. 13 copyright 2021, Elsevier Ltd.

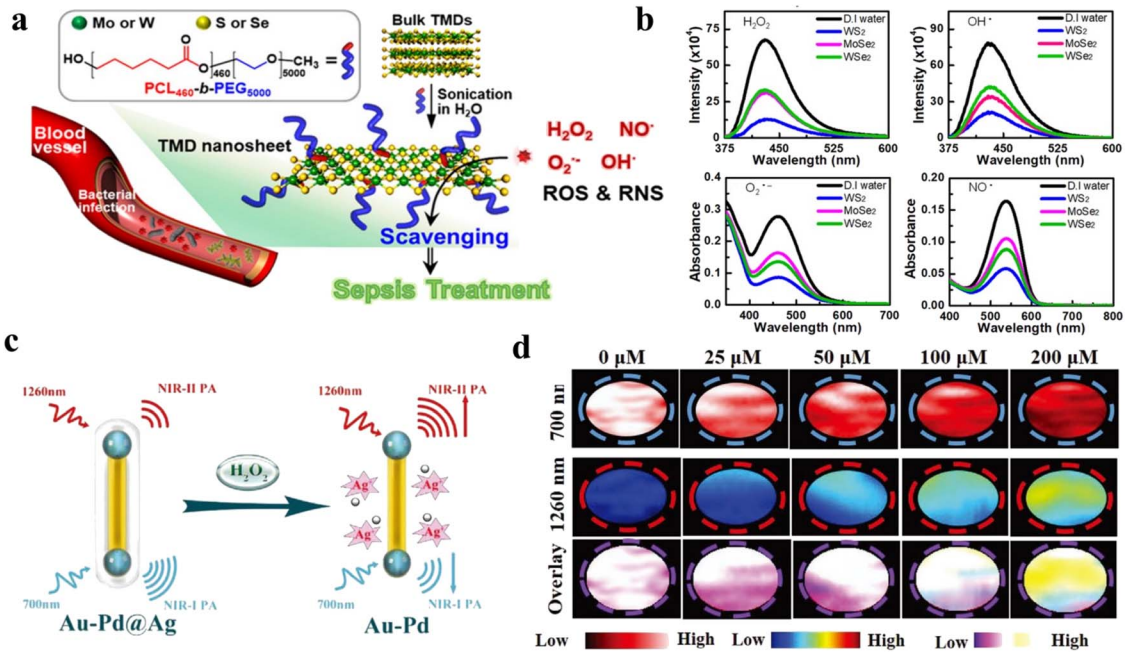

Fig. 11 (a) Schematic illustration of two-dimensional transition-metal dichalcogenides for inflammatory treatment. Reproduced from ref. 32 copyright 2020, American Chemical Society. (b) The clearing of ROS and RNS by 2D-TMD. Reproduced from ref. 32 copyright 2020, American Chemical Society. (c) Schematic illustration of Au–Pd@Ag nanorods for detection of H_2O_2 by PA imaging. Reproduced from ref. 34 copyright 2020, WILEY-VCH Verlag GmbH & Co. KGaA, Weinheim. (d) PA intensity of 700 nm and 1260 nm at different hydrogen peroxide concentrations. Reproduced from ref. 34 copyright 2020, WILEY-VCH Verlag GmbH & Co. KGaA, Weinheim.

SDT. Moreover, H_2O_2 could be also used to directly generate ˙OH for antibacterial therapy.[192] For example, Yang *et al.* designed Cu_2O nanoparticles, which catalyzed H_2O_2 to ˙OH by a Fenton-like reaction (Fig. 9d).[193] The oxidative stress caused by ˙OH could induce bacterial death. Then, Cu_2O nanoparticles could be transformed to Cu_9S_8 NPs in bacterial environment, which as photoacoustic agents accurately distinguished between bacterial infections and normal tissues (Fig. 9e). After injection of Cu_2O NPs, photoacoustic signal in normal tissue did not change significantly. However, Cu_2O NPs could be vulcanized to form Cu_9S_8 NPs in the infected tissue, the PA signal intensity reached the maximum after *in situ* injection at 12 h.

Similar to ˙OH, nitric oxide (NO) as a broad-spectrum antibacterial molecule could also be used for antibacterial therapy.[194] In the presence of H_2O_2, L-arginine could be oxidized to produce NO.[194] Zhu *et al.* designed a nanoplatform Ce6@Arg-ADP, which had rich L-arginine, to deal with bacteria.[33] The PDT could control generation of NO *in situ* and substantially promoted wound healing (Fig. 9f). As shown in Fig. 9g, there was almost no NO produced in PBS + laser-, Ce6@Arg-ADP-, Ce6 + laser-, Ce6@Lys-ADP + laser-treated bacteria, but large amount of NO was observed in Ce6@Arg-ADP + laser-treated bacteria. As displayed in Fig. 9h, at all tested concentrations, the antibacterial effect of Ce6@Arg-ADP + laser was significantly higher than that of Ce6 + laser and Ce6@Lys-ADP + laser. In the treatment of abscess, it was necessary to control infection, promote the rapid healing of disfigured wound, shorten the time of wound care, and avoid secondary infection. The result in Fig. 9i, Ce6@Arg-ADP + laser could inhibit bacterial infection and promote wound healing. Consequently, H_2O_2-based antibacterial treatment and imaging strategies provide an excellent method for further biomedical application.

4.3 Dental diseases therapy by producing ROS and correlated diagnosis

Dental microbial biofilms, which can embed microorganisms, are the causative factor of dental diseases, such as dental caries and periodontitis.[195,196] Because the entire biofilm is protected by a homegrown organic polymer matrix, it is more resistant to treatment than free bacteria.[196] Previously, ˙OH generation from H_2O_2 could disrupt dental microbial biofilms were reported.[196] Therefore, H_2O_2-related dental disease treatment and diagnosis receive more attention. For instance, Villa *et al.* synthesized self-propelled tubular microrobots to disrupt biofilms by the generation of bubbles and ˙OH (Fig. 10a).[196] As shown in Fig. 10b, the motion mechanism was the decomposition of H_2O_2 into O_2 catalyzed by Pt NPs on the inner surface. Then, this caused O_2 exit from one end of the tube, which triggers its motion in the opposite direction. At the same time, it was not difficult to find from Fig. 10c that microrobots motion velocity was increased with the increase of H_2O_2 concentration. Thus, the self-propelled tubular microrobot could destroy biofilms in the presence of H_2O_2. Huang *et al.* designed Dex-IONP-GOx nanoplatforms to generate ˙OH from H_2O_2 for disrupting biofilms.[13] As shown in Fig. 10d, this nanoplatform had cascade catalysis activity to continuously produce H_2O_2 and ˙OH for the prevention of dental caries. Furthermore, this study found that

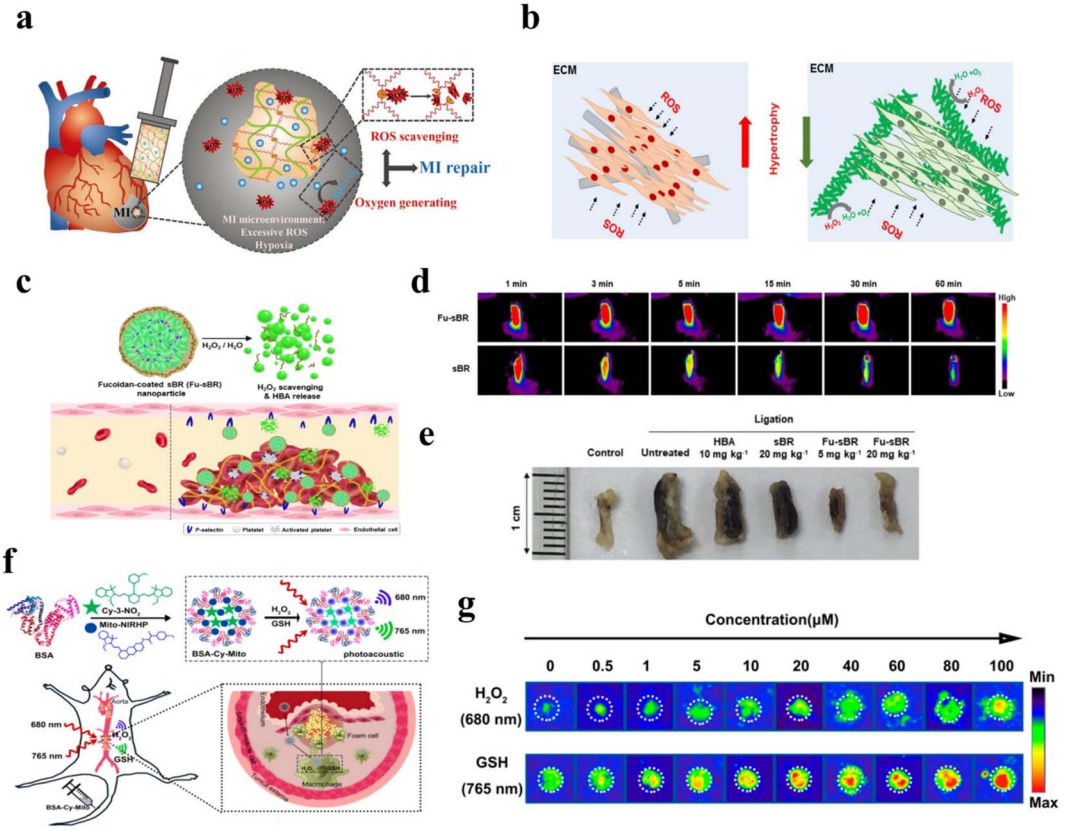

Fig. 12 (a) Schematic illustration of hydrogel for H_2O_2-scavenging and O_2 generating. Reproduced from ref. 209 copyright 2020, Wiley-VCH GmbH. (b) Schematic illustration of nanofiber for mitigating H_2O_2 generated after myocardial infarction. Reproduced from ref. 210 copyright 2020, Elsevier B.V. (c) Schematic illustration of Fu-sBR nanoassemblies for antithrombotic treatment. Reproduced from ref. 211 copyright 2021, Wiley-VCH GmbH. (d) Fluorescence images of thrombosed IVC excised at 60 min after injection. Reproduced from ref. 211 copyright 2021, Wiley-VCH GmbH. (e) Photographs of thrombosed IVC excised at 48 h after the release of ligation. Reproduced from ref. 211 copyright 2021, Wiley-VCH GmbH. (f) Schematic illustration of nanoprobe to detect H_2O_2 for atherosclerotic plaque vulnerability assessment. Reproduced from ref. 212 copyright 2019, American Chemical Society. (g):PA imaging of BSA-Cy-Mito nanoprobe with different concentrations of H_2O_2 and GSH. Reproduced from ref. 212 copyright 2019, American Chemical Society.

the Dex-IONP-GOx nanoplatform had specific binding to S. mutans, which has destructive effect on biofilm (Fig. 10e). Therapeutic effect evaluation of dental disease has also been developed recently.[197] Wang *et al.* designed copper oxide nanoparticles anchoring onto black phosphorus nanosheets for assessment of disease progression and treatment effectiveness.[197] This nanoplatform possessed superior selectivity, it could utilize human gingival crevicular fluid and saliva samples for the diagnosis of periodontitis.

4.4 Enhanced therapy and imaging by direct consumption of H_2O_2

4.4.1 Inflammations therapy and correlated imaging. Inflammation plays a pathological basis role in multiple chronic diseases.[34] Previous studies have shown that H_2O_2 can be produced in inflammation areas and kill infiltrating pathogens.[34] However, oxidative stress caused by excess H_2O_2 will exacerbate the inflammatory response and impede the repair of tissues and organs.[198] Oxidative stress of H_2O_2 damages endothelial barrier, promotes migration and infiltration of inflammatory cells, and aggravates tissue damage.[199] Therefore, the reduction of H_2O_2 is one of the effective ways for anti-inflammatory treatment. For example, Yim *et al.* designed two-dimensional (2D) transition-metal dichalcogenides (2D-TMD), which could scavenge intracellular H_2O_2 for inflammatory treatment (Fig. 11a).[32] As described in Fig. 11b, the nanomaterial had a good ability to clear ROS and reactive nitrogen species (RNS), which could alleviate the inflammatory response to a large extent. Additionally, a H_2O_2-responsive nanoplatforms which released drugs and CO_2 gas treatment for inflammation inhibition have been reported.[200]

More than that, imaging can be used to assess changes in H_2O_2 concentration in the inflamed area, enabling monitoring of therapeutic effects and inflammatory progression.[201,202] Li *et al.* designed a novel nanotheranostic agent (TMSN@PM) to scavenge the excess ROS for alleviating inflammation and release Mn^{2+} ions.[203] The number of Mn^{2+} ions released was correlated with the ROS level, which could be monitored by MRI. Moreover, Ye *et al.* designed a H_2O_2-responsive nanomaterial (Au–Pd@Ag nanorod) to detect H_2O_2 by PAI (Fig. 11c).[34] The PAI signal at 1260 nm and 700 nm could be used accurately differentiate the inflammation region and normal tissue in

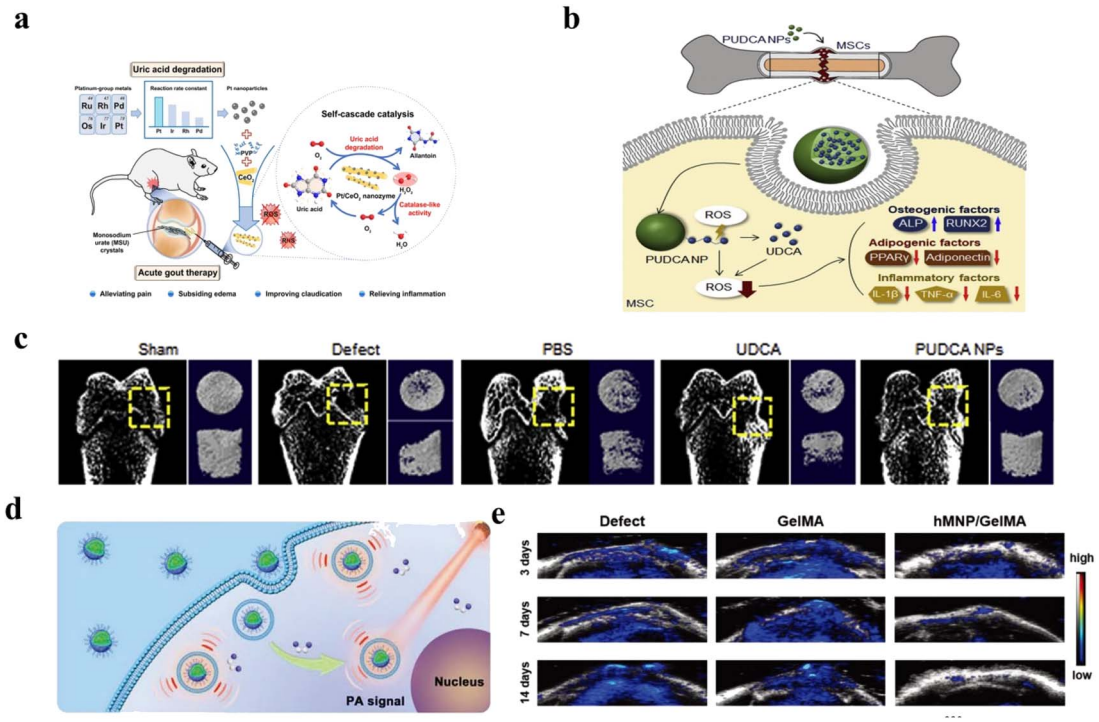

Fig. 13 (a) Schematic illustration of synthesis and nanozyme activities of Pt/CeO_2 for treatment of acute gout. Reproduced from ref. 230 copyright 2022, American Chemical Society. (b) Schematic illustration of PUDCA NPs for bone tissue regeneration. Reproduced from ref. 5 copyright 2020, Elsevier B.V. (c) CT images after different treatments. Reproduced from ref. 5 copyright 2020, Elsevier B.V. (d) Schematic illustration of Lipo@HRP&ABTS nanoprobes for PAI. Reproduced from ref. 234 copyright 2021, Wiley-VCH GmbH. (e) The PA signal of Lipo@HRP&ABTS nanoprobes to detect H_2O_2. Reproduced from ref. 234 copyright 2021, Wiley-VCH GmbH.

Fig. 11d. In another study, a nanoparticle that could be responsive to H_2O_2 to produce CO_2 bubbles for USI has been developed.[204] And a Co complex has been designed for detection of H_2O_2 production by MRI.[205] Utilizing the large change in chemical shift shown at ^{19}F when oxidizing from Co(II) to Co(III), this was done using a chemical shift selective pulse train. Furthermore, H_2O_2-responsive nanomaterials have also been shown to be useful in the treatment and diagnosis of other inflammatory diseases, including inflammation of musculoskeletal systems, interstitial cystitis, ulcerative colitis, lupus nephritis, *etc.*[176,206–208] In a word, H_2O_2-responsive nanomaterials offer an alternative strategy for inflammation therapy and diagnosis.

4.4.2 Cardiovascular diseases therapy and correlated imaging. In the cardiovascular system, H_2O_2-responsive nanomaterials can be used for the treatment and imaging of many diseases, such as thrombosis.[213] Myocardial infarction (MI), a cardiac disease, has a high mortality rate in the world.[214] A hypoxic microenvironment in MI tissues will induce aberrant production of H_2O_2.[215] Unfortunately, excessive H_2O_2 will lead to myocardial damage, which is adverse to cardiac repair after MI.[209] Therefore, scavenging of H_2O_2 and production of O_2 means a potential way for MI repair. Ding *et al.* synthesized a hydrogel, that contained CAT, to turn H_2O_2 into O_2.[209] As depicted in Fig. 12a, this hydrogel possessed excellent properties to scavenge H_2O_2 for MI repair. Experimental results showed that removing H_2O_2 was beneficial to MI repair. Moreover, cardiac hypertrophy is also associated with H_2O_2, which is caused by MI, leading to cardiac failure.[216,217] Inspired by this, a nanofiber has been developed to scavenge H_2O_2 for cardiac hypertrophy inhibition as shown in Fig. 12b.[210] In addition, H_2O_2-related nanotechnology could also be used for early cardiac disease diagnosis, such as early acute myocardial infarction.[218]

Similarly, H_2O_2-related nanotechnology has been widely used in vascular systems, such as thrombus and angiogenesis.[219,220] It has been reported that the pathophysiological process of thrombus is associated with H_2O_2.[221,222] The generation of H_2O_2 was associated with activated platelets and injured endothelium.[223] Platelet-dependent thrombus formation could be progressed by high levels of H_2O_2.[224] Herein, the removal of overproduced H_2O_2 was an effective method for thrombosis treatment. Jung *et al.* synthesized H_2O_2-responsive Fu-sBR nano assemblies to scavenge H_2O_2 (Fig. 12c).[211] This nanomaterial possessed the ability for targeted on-demand treatment of thrombus. As shown in Fig. 12d and e, due to the H_2O_2-responsive effect of Fu-sBR, there was no attenuation of the fluorescence signal within 60 min. However, sBR was not H_2O_2-responsive effect, and the fluorescence signal continued to decay. Photographs of thrombosed excised at 48 h, Fu-sBR had a good effect on the treatment of thrombus. In another study, Gao *et al.* designed a nanoprobe to detect H_2O_2 for atherosclerotic plaque vulnerability assessment by PAI and precise treatment in Fig. 12f.[212] As described in Fig. 12g, the PAI signal of

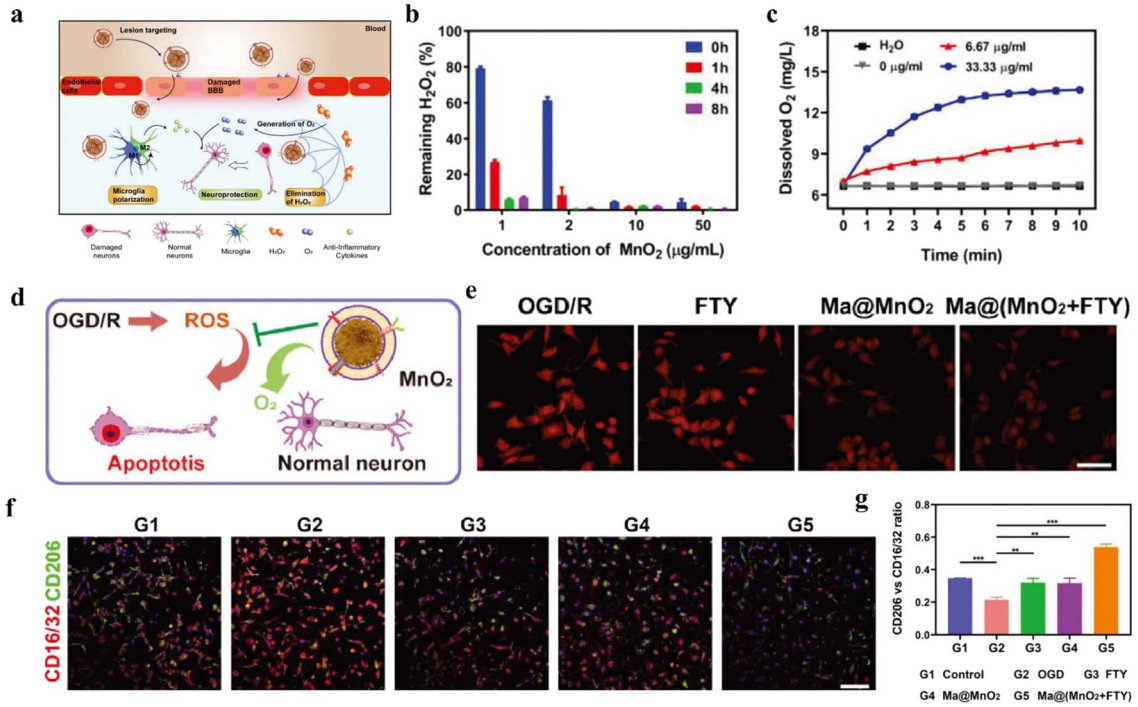

Fig. 14 (a) Schematic illustration of Ma@(MnO_2 + FTY) nanoparticles to protect damaged neurons. (b) The concentration of H_2O_2 with different concentration of MnO_2. (c) The concentration of O_2 with different concentration of MnO_2. (d) Scheme of the mechanism of neuroprotection by Ma@MnO_2 nanospheres on OGD/R. (e) Fluorescence images of intracellular oxygen concentration after different treatments. (f) Immunostained images of microglia with CD16/32 and CD206. (g) Quantification of the relative fluorescence intensity of CD206 *versus* CD16/32. (a–g) Reproduced under terms of the CC-BY license.[238] Copyright 2021, C. Li *et al.*, Published by Wiley-VCH GmbH.

nanoprobe increased with the increase of H_2O_2 concentration. Furthermore, the H_2O_2-responsive nanoplatform has been proven to release drugs in the blood vessels.[223,225–227] Therefore, these H_2O_2-related nanoplatforms offered excellent opportunities for future cardiovascular disease applications.

4.4.3 Bone injury therapy and correlated imaging. High ROS levels, a character of bone tissue injury, can promote osteoclast generation.[228] H_2O_2, as a representative type of ROS, can induce oxidative stress, which is detrimental to bone injury repair.[229] Therefore, nanotechnology to remove H_2O_2 provides a potential method for treatment of bone injury.

Lin *et al.* synthesized a Pt/CeO_2 nanozyme for the treatment of monosodium urate (MSU)-induced acute gout.[230] As shown in Fig. 13a, nanosized Pt as a uricase and CAT mimic could scavenge uric acid and H_2O_2. The Pt/CeO_2 nanozyme catalyzed uric acid and O_2 to H_2O_2 and water-soluble allantoin, which reduced the production of the tophus. Then, the CAT mimic could provide a constant supply of oxygen, which creates a cycle of uric acid removal. Thus, the nanozyme alleviated joint pain and tissue injury. According to previous researches, peroxalate ester linkage was reported that it could also to react with H_2O_2.[231] Inspired by this, peroxalate ester-based PUDCA NPs have been synthesized to scavenge H_2O_2 and release ursodeoxycholic acid (UDCA) for promoting the osteogenic differentiation of mesenchymal stem cells (MSCs).[5] As described in Fig. 13b, UDCA could be released in the presence of H_2O_2, followed by it scavenged H_2O_2 for bone tissue regeneration. This research also proved that reducing levels of H_2O_2 could decrease the adipogenic differentiation of MSCs, and then reduce the inhibition of bone regeneration. By micro-computed tomography analysis, PUDCA NP-treated group had the best effect on bone injury repair in Fig. 13c. In a similar study, Zhang *et al.* focused on improving the activity of MSCs and osteogenic differentiation.[232] Fe_3O_4@GO/BMP2 magnetic nanocomposites could reduce H_2O_2 by Fenton reaction and capture $^{\cdot}OH$ for bone tissue regeneration under magnetic regulation.

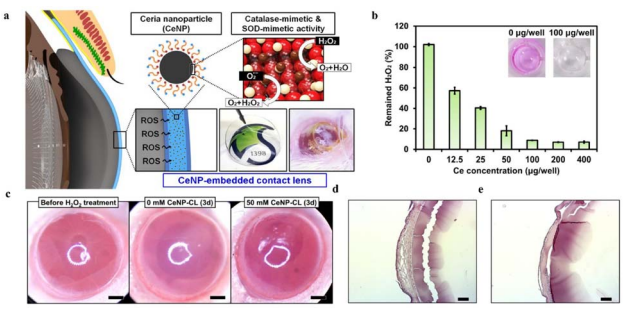

Fig. 15 (a) Schematic illustration of CeNP-CL for scavenging the ROS on the cornea (b) changes of H_2O_2 at different Ce concentrations. (c) Representative photographs of the ocular surface for different groups. (d) Histologic photographs for the group wearing 0 mM CeNP-CLs. (e) Histologic photographs for the group wearing 50 mM CeNP-CLs. Reproduced from ref. 245 copyright 2020, American Chemical Society.

More than that, H_2O_2-responsive nanomaterials have been proven to promote osteogenesis.[233] Because of this, Li *et al.* designed hollow manganese dioxide nanoparticles (hMNPs)/gelatin methacryloyl (GelMA) composite hydrogels to clear H_2O_2 and release Mn^{2+} for promoting bone regeneration.[234] MnO_2 NPs released Mn^{2+} in response to H_2O_2, and then Mn^{2+} promoted cell growth and osteogenic differentiation. In order to further study the concentration of H_2O_2 in the bone injury area, Lipo@HRP&ABTS nanoprobe was introduced in this experiment (Fig. 13d). In the presence of H_2O_2, Lipo@HRP&ABTS nanoprobe had strong NIR absorption, which could be converted into PA signal, realizing real-time imaging monitoring of H_2O_2 (Fig. 13e). In a word, H_2O_2-related nanoparticles had marvelous prospects in the treatment and diagnosis of bone injury.

4.4.4 Neurologic diseases therapy and correlated imaging. H_2O_2-induced cellular oxidation was not conducive to neurologic injury repair caused by diseases, such as neuroinflammation, traumatic brain injury, Parkinson's disease, and ischemic stroke.[30,36,235,236] The production of H_2O_2 was related to reperfusion after ischemia stroke, and the oxidative stress generated by H_2O_2 would further aggravate the severity of ischemia stroke.[237] According to previous researches, scavenging excessive H_2O_2 could effectively retard the progression of neuronal death caused by an ischemic stroke.[237] Inspired by this, Li *et al.* designed a macrophage-disguised fingolimod (FTY)-loaded MnO_2 nanoparticles (Ma@(MnO_2 + FTY)) nanoparticle to convert H_2O_2 to O_2 in the ischemic brain.[238] As depicted in Fig. 14a, the nanoparticle could polarity M1 type microglia (proinflammatory type) to M2 type (anti-inflammatory), then cooperated with decomposing H_2O_2 and generating O_2 to protect damaged neurons. As described in Fig. 14b and c, Ma@(MnO_2 + FTY) NPs could remove H_2O_2 while producing O_2, which was important for the protection of nerve cells. And oxygen-glucose deprivation/reoxidation (OGD/R) mimicked neuronal ischemia-reperfusion, demonstrating that ROS could be removed as a major source of nerve damage (Fig. 14d). Subsequently, $[(Ru(dpp)_3)]Cl_2$ probe was used to study the intracellular O_2 concentration, which proved that Ma@(MnO_2 + FTY) NPs could also produce a large amount of O_2 in the cell (Fig. 14e). Immunofluorescence results showed that OGD/R increased the expression of M1 marker CD16/32, and FTY and Ma@MnO_2 nanoparticles could decrease the expression of CD16/32 and increase the expression of M2 marker CD206 (Fig. 14f). Because it was a significant molecule in neurologic injury repair, change in H_2O_2 levels was closely related to the progression of diseases.[239] Wang *et al.* designed a nanoprobe based on a PCAB for detecting H_2O_2 *in vivo*.[240] A fluorescent imaging probe CRANAD-88 has been created to investigate H_2O_2 in Alzheimer's disease (AD) brains.[241] Qiao *et al.* have also done some research on H_2O_2-responsive nanomaterials for the treatment of AD.[242] Therefore, H_2O_2-related treatment and diagnosis have shown potential methods for neurologic diseases.

4.4.5 Ophthalmic diseases therapy. It has been proved that some ophthalmic diseases were related to the increasing levels of H_2O_2.[243] In ocular diseases, the overexpress production of H_2O_2 was based the prooxidative/antioxidative cellular imbalance.[243] The overexpress production of H_2O_2 could disrupt retinal homeostasis, which is one of the cause of uveitis.[35] Not only that, the human eye is more susceptible to oxidative damage, especially to the cornea, because of its exposure to environment.[244] As the ocular surface composition, antioxidative damage of cornea is an essential content for the treatment of ophthalmic diseases.[244] Therefore, Choi and coworkers designed a ROS-scavenging ceria nanoparticle-embedded contact lens (CeNP-CLs) for scavenging the ROS on the cornea.[245] As reflected in Fig. 15a, CeNP-CLs possessed CAT-like ability and SOD-mimetic activities, which could remove H_2O_2 and other ROS. With the increase of Ce concentration, the concentration of H_2O_2 continued to decrease (Fig. 15b). Corneal endothelial damage caused by H_2O_2 infiltration will lead to corneal opacity. As described in Fig. 15c, obvious corneal opacity could be found in the group with 0 mM CeNP-CLs after 3 days of H_2O_2 exposure, compared with before H_2O_2 exposure. According to the tissue sections, the degree of corneal epithelial injury in the group wearing 0 mM CeNP-CLs (Fig. 15d) was greater than that in the group wearing 50 mM CeNP-CLs (Fig. 15e). These findings suggested that adequate clearance of H_2O_2 in the presence of CeNPs-CLs can reduce damage to corneal epithelium and endothelial cells. To sum up, H_2O_2-related nanoparticles have marvelous prospects and potential in the treatment and diagnosis of many diseases.

5 Conclusion and perspective

H_2O_2-responsive nanomaterials with their applications have been proven as interesting and meaningful methods for disease diagnosis and therapy. On the one hand, under external light or US excitation, the O_2 generated from the decomposition of H_2O_2 by the H_2O_2-responsive nanomaterials is converted into ROS for disease treatment. Hypoxia could also be alleviated by the generation of O_2, which enhanced the effectiveness of therapy. On the other hand, H_2O_2-responsive nanomaterials can catalyze H_2O_2 into $^{\bullet}OH$ by Fenton or Fenton-like reaction. Furthermore, the combination of multiple treatments has also become a hot research topic. Treatment is often used in conjunction with other treatment modalities for increasing the effect, which possessed a "1 + 1 > 2" treatment effect. More importantly, imaging-guided therapy has been reported to could monitor the effect of H_2O_2-related treatments in real-time. This is mainly based on the fact that nanomaterials can react with H_2O_2 and enhance imaging signal. In this review, we summarized recent advances in H_2O_2-responsive nanomaterials and their applications in treatment and diagnosis of multiple types of diseases, including tumors, bacterium, dental diseases, inflammations, cardiovascular diseases, bones, neurologic diseases and ophthalmic diseases. According to the mechanism of therapy, they can be divided into two different groups: (1) producing ROS and (2) consuming H_2O_2.

Despite some advantages of H_2O_2-responsive nanomaterials and their related diagnosis and treatment approaches, many challenges are still needed to be addressed. (1) Most H_2O_2-responsive sensitizers or nanomaterials possess potential

toxicity; (2) the synthesis process of H_2O_2-responsive nanomaterials is tedious and complex; (3) the researches on H_2O_2-related nontumor diseases therapy are not in-depth and comprehensive enough; (4) the effectiveness of some nanoplatforms still needs further improvement.

As a novel and versatile theranostic modality, H_2O_2-responsive nanomaterials have shown their high specificity and therapeutic performances in various biomedical applications, opening up new avenues for the treatment and diagnosis of H_2O_2 overexpression diseases. Provided the above challenges are adequately addressed, this unique H_2O_2-responsive nanomaterial is expected to enter the clinical stage in the near future to bring benefit to personalized biomedicine. Therefore, we hope that this review can contribute to providing new design inspirations and application ideas for various functional nanomaterials related to H_2O_2.

Conflicts of interest

There are no conflicts to declare.

Acknowledgements

We gratefully acknowledge support from the National Natural Science Foundation of China (No. 82102056) and the Natural Science Foundation of Fujian Province of China (No. 2022J01280).

Notes and references

1 A. Adrian, K. Schoppmann, J. Sromicki, S. Brungs, M. von der Wiesche, B. Hock, W. Kolanus, R. Hemmersbach and O. Ullrich, *Cell Commun. Signal.*, 2013, **11**, 98.
2 H. Sies and D. P. Jones, *Nat. Rev. Mol. Cell Biol.*, 2020, **21**, 363–383.
3 P. Wang, W. Yang, S. Shen, C. Wu, L. Wen, Q. Cheng, B. Zhang and X. Wang, *ACS Nano*, 2019, **13**, 11168–11180.
4 L. Meng, Y. Cheng, X. Tong, S. Gan, Y. Ding, Y. Zhang, C. Wang, L. Xu, Y. Zhu, J. Wu, Y. Hu and A. Yuan, *ACS Nano*, 2018, **12**, 8308–8322.
5 Y. Arai, H. Park, S. Park, D. Kim, I. Baek, L. Jeong, B. J. Kim, K. Park, D. Lee and S. H. Lee, *J. Control Release.*, 2020, **328**, 596–607.
6 Q. Zeng, R. Zhang, T. Zhang and D. Xing, *Biomaterials*, 2019, **207**, 39–48.
7 Q. Jia, J. Ge, W. Liu, X. Zheng, S. Chen, Y. Wen, H. Zhang and P. Wang, *Adv. Mater.*, 2018, **30**, e1706090.
8 Y. Hu, W. Wang, S. Huang, J. Li, Y. Zhang, Y. Gao, Y. Cheng, Z. Wu and X. Zhang, *Chem. Eng. J.*, 2022, **431**, 133704.
9 S. Wang, R. Tian, X. Zhang, G. Cheng, P. Yu, J. Chang and X. Chen, *Adv. Mater.*, 2021, **33**, e2007488.
10 H. Ranji-Burachaloo, P. A. Gurr, D. E. Dunstan and G. G. Qiao, *ACS Nano*, 2018, **12**, 11819–11837.
11 M. Lopez-Lazaro, *Cancer Lett.*, 2007, **252**, 1–8.
12 X. Hou, H. Zeng, X. Chi and X. Hu, *Nano Lett.*, 2021, **21**, 9966–9975.
13 Y. Huang, Y. Liu, S. Shah, D. Kim, A. Simon-Soro, T. Ito, M. Hajfathalian, Y. Li, J. C. Hsu, L. M. Nieves, F. Alawi, P. C. Naha, D. P. Cormode and H. Koo, *Biomaterials*, 2021, **268**, 120581.
14 P. Niu, J. Liu, F. Xu, L. Yang, Y. Li, A. Sun, L. Wei, X. Liu and X. Song, *ACS Appl. Bio Mater.*, 2022, **5**, 1683–1691.
15 K. Zamojc, M. Zdrowowicz, D. Jacewicz, D. Wyrzykowski and L. Chmurzynski, *Crit. Rev. Anal. Chem.*, 2016, **46**, 171–200.
16 L. H. Fu, C. Qi, J. Lin and P. Huang, *Chem. Soc. Rev.*, 2018, **47**, 6454–6472.
17 M. Alfonso-Prieto, X. Biarnes, P. Vidossich and C. Rovira, *J. Am. Chem. Soc.*, 2009, **131**, 11751–11761.
18 Y. Sheng, I. A. Abreu, D. E. Cabelli, M. J. Maroney, A. F. Miller, M. Teixeira and J. S. Valentine, *Chem. Rev.*, 2014, **114**, 3854–3918.
19 W. Yang, X. Shi, Y. Shi, D. Yao, S. Chen, X. Zhou and B. Zhang, *ACS Nano*, 2018, **12**, 12169–12180.
20 D. He, L. Hai, X. He, X. Yang and H.-W. Li, *Adv. Funct. Mater.*, 2017, **27**, 1704089.
21 M. Chang, M. Wang, M. Wang, M. Shu, B. Ding, C. Li, M. Pang, S. Cui, Z. Hou and J. Lin, *Adv. Mater.*, 2019, **31**, e1905271.
22 X. Wang, T. Xiong, M. Cui, X. Guan, J. Yuan, Z. Wang, R. Li, H. Zhang, S. Duan and F. Wei, *Appl. Mater. Today*, 2020, **21**, 100827.
23 D. Wang, H. Wu, S. Z. F. Phua, G. Yang, W. Qi Lim, L. Gu, C. Qian, H. Wang, Z. Guo, H. Chen and Y. Zhao, *Nat. Commun.*, 2020, **11**, 357.
24 Y. Cheng, C. Wen, Y. Q. Sun, H. Yu and X. B. Yin, *Adv. Funct. Mater.*, 2021, **31**, 2104378.
25 F. Nan, Q. Jia, X. Xue, S. Wang, W. Liu, J. Wang, J. Ge and P. Wang, *Biomaterials*, 2022, **284**, 121495.
26 J. Ding, G. Lu, W. Nie, L. L. Huang, Y. Zhang, W. Fan, G. Wu, H. Liu and H. Y. Xie, *Adv. Mater.*, 2021, **33**, e2005562.
27 S. Y. Liu, Y. Xu, H. Yang, L. Liu, M. Zhao, W. Yin, Y. T. Xu, Y. Huang, C. Tan, Z. Dai, H. Zhang, J. P. Zhang and X. M. Chen, *Adv. Mater.*, 2021, **33**, e2100849.
28 S. Fu, R. Yang, J. Ren, J. Liu, L. Zhang, Z. Xu, Y. Kang and P. Xue, *ACS Nano*, 2021, **15**, 11953–11969.
29 J. Wang, J. Huang, W. Zhou, J. Zhao, Q. Peng, L. Zhang, Z. Wang, P. Li and R. Li, *J. Nanobiotechnol.*, 2021, **19**, 87.
30 S. K. Rajendrakumar, V. Revuri, M. Samidurai, A. Mohapatra, J. H. Lee, P. Ganesan, J. Jo, Y.-K. Lee and I.-K. Park, *Nano Lett.*, 2018, **18**, 6417–6426.
31 D. Mao, F. Hu, Kenry, S. Ji, W. Wu, D. Ding, D. Kong and B. Liu, *Adv. Mater.*, 2018, **30**, e1706831.
32 D. Yim, D. E. Lee, Y. So, C. Choi, W. Son, K. Jang, C. S. Yang and J. H. Kim, *ACS Nano*, 2020, **14**, 10324–10336.
33 J. Zhu, J. Tian, C. Yang, J. Chen, L. Wu, M. Fan and X. Cai, *Small*, 2021, **17**, e2101495.
34 J. Ye, Z. Li, Q. Fu, Q. Li, X. Zhang, L. Su, H. Yang and J. Song, *Adv. Funct. Mater.*, 2020, **30**, 2001771.
35 G. Wang, X. Li, N. Li, X. Wang, S. He, W. Li, W. Fan, R. Li, J. Liu and S. Hou, *Redox Biol.*, 2022, **52**, 102297.
36 Y. Liu, K. Ai, X. Ji, D. Askhatova, R. Du, L. Lu and J. Shi, *J. Am. Chem. Soc.*, 2017, **139**, 856–862.

37 S. Gao, G. Wang, Z. Qin, X. Wang, G. Zhao, Q. Ma and L. Zhu, *Biomaterials*, 2017, **112**, 324–335.
38 Y. Tian, H. Zhou, Q. Cheng, H. Dang, H. Qian, C. Teng, K. Xie and L. Yan, *J. Mater. Chem. B*, 2022, **10**, 707–716.
39 W. Liu, S. Y. Yin, Y. Hu, T. Deng and J. Li, *ACS Appl. Mater. Interfaces*, 2022, **14**, 2629–2637.
40 X. Chen, X. Ren, L. Zhang, Z. Liu and Z. Hai, *Anal. Chem.*, 2020, **92**, 14244–14250.
41 T. Liu, N. Zhang, Z. Wang, M. Wu, Y. Chen, M. Ma, H. Chen and J. Shi, *ACS Nano*, 2017, **11**, 9093–9102.
42 Q. Chen, C. Liang, X. Sun, J. Chen, Z. Yang, H. Zhao, L. Feng and Z. Liu, *Proc. Natl. Acad. Sci. U. S. A.*, 2017, **114**, 5343–5348.
43 C. Cheng, Y. Gao, W. Song, Q. Zhao, H. Zhang and H. Zhang, *Chem. Eng. J.*, 2020, **380**, 140049.
44 Q. Pan, B. Zhang, X. Peng, S. Wan, K. Luo, W. Gao, Y. Pu and B. He, *Chem. Commun.*, 2019, **55**, 13896–13899.
45 C. Yik-Sham Chung, G. A. Timblin, K. Saijo and C. J. Chang, *J. Am. Chem. Soc.*, 2018, **140**, 6109–6121.
46 J. F. Mukerabigwi, W. Yin, Z. Zha, W. Ke, Y. Wang, W. Chen, A. Japir, Y. Wang and Z. Ge, *J. Control Release.*, 2019, **303**, 209–222.
47 Q. Zeng, R. Zhang, T. Zhang and D. Xing, *Biomaterials*, 2019, **207**, 39–48.
48 Z. W. Wang, D. Su, X. Q. Li, J. J. Cao, D. C. Yang and J. Y. Liu, *Molecules*, 2018, **24**, 32.
49 M. C. Chang, A. Pralle, E. Y. Isacoff and C. J. Chang, *J. Am. Chem. Soc.*, 2004, **126**, 15392–15393.
50 J. Wang, J. Liu, D. Q. Lu, L. Chen, R. Yang, D. Liu and B. Zhang, *Carbohydr. Polym.*, 2022, **292**, 119699.
51 Y. J. Jo, M. Gulfam, S. H. Jo, Y. S. Gal, C. W. Oh, S. H. Park and K. T. Lim, *Carbohydr. Polym.*, 2022, **286**, 119303.
52 J. Yang, S. Pan, S. Gao, T. Li and H. Xu, *Biomaterials*, 2021, **271**, 120721.
53 D. Pham, U. Basu, I. Pohorilets, C. M. St Croix, S. C. Watkins and K. Koide, *Angew Chem. Int. Ed. Engl.*, 2020, **59**, 17435–17441.
54 S. Ye, J. J. Hu and D. Yang, *Angew Chem. Int. Ed. Engl.*, 2018, **57**, 10173–10177.
55 B. Dong, X. Song, X. Kong, C. Wang, Y. Tang, Y. Liu and W. Lin, *Adv. Mater.*, 2016, **28**, 8755–8759.
56 N. Soh, O. Sakawaki, K. Makihara, Y. Odo, T. Fukaminato, T. Kawai, M. Irie and T. Imato, *Bioorg. Med. Chem.*, 2005, **13**, 1131–1139.
57 H. Ding, Y. Cai, L. Gao, M. Liang, B. Miao, H. Wu, Y. Liu, N. Xie, A. Tang, K. Fan, X. Yan and G. Nie, *Nano Lett.*, 2019, **19**, 203–209.
58 P. Campomanes, U. Rothlisberger, M. Alfonso-Prieto and C. Rovira, *J. Am. Chem. Soc.*, 2015, **137**, 11170–11178.
59 X. Qin, C. Wu, D. Niu, L. Qin, X. Wang, Q. Wang and Y. Li, *Nat. Commun.*, 2021, **12**, 5243.
60 F. P. Chang, Y. P. Chen and C. Y. Mou, *Small*, 2014, **10**, 4785–4795.
61 Y. Fujiki and M. C. Bassik, *Trends Cell Biol.*, 2021, **31**, 148–151.
62 B. K. Vainshtein, W. R. Melik-Adamyan, V. V. Barynin, A. A. Vagin and A. I. Grebenko, *Nature*, 1981, **293**, 411–412.
63 S. Z. F. Phua, G. Yang, W. Q. Lim, A. Verma, H. Chen, T. Thanabalu and Y. Zhao, *ACS Nano*, 2019, **13**, 4742–4751.
64 Q. Chen, J. Chen, Z. Yang, J. Xu, L. Xu, C. Liang, X. Han and Z. Liu, *Adv. Mater.*, 2019, **31**, e1802228.
65 H. Phan, R. Cavanagh, D. Destouches, F. Vacherot, B. Brissault, V. Taresco, J. Penelle and B. Couturaud, *ACS Appl. Polym. Mater.*, 2022, **4**, 7778–7789.
66 S. Park, J. Yoon, S. Bae, M. Park, C. Kang, Q. Ke, D. Lee and P. M. Kang, *Biomaterials*, 2014, **35**, 5944–5953.
67 K. Ou, Y. Kang, L. Chen, X. Zhang, X. Chen, Y. Zheng, J. Wu and S. Guan, *Biomater. Sci.*, 2019, **7**, 2491–2498.
68 Z. Lu, J. Zhang, W. Yin, C. Guo and M. Lang, *Macromol. Rapid Commun.*, 2022, **43**, e2200156.
69 T. Liu, J. Tian, L. Cui, Q. Liu, L. Wu and X. Zhang, *Colloids Surf. B Biointerfaces*, 2019, **178**, 137–145.
70 Z. Wang, L. Zhang and Y. Tian, *Analyst*, 2015, **140**, 3788–3793.
71 C. Ren, L. Chu, F. Huang, L. Yang, H. Fan, J. Liu and C. Yang, *RSC Adv.*, 2017, **7**, 1313–1317.
72 X. Guo, Y. Li, Y. Li, Z. Ye, J. Zhang, T. Zhu and F. Li, *Electrochim. Acta*, 2020, **354**, 136763.
73 Z. Qu, D. Zhang, C. Wang, S. Tian, Y. Deng, D. Qin and H. Duan, *Polymers*, 2022, **14**, 3005.
74 X. Shang, S. He, Z. Xu, W. Lu and W. Zhang, *Electroanalysis*, 2021, **33**, 1088–1095.
75 W. Wu, L. Huang, E. Wang and S. Dong, *Chem. Sci.*, 2020, **11**, 9741–9756.
76 Y. Fan, S. Liu, Y. Yi, H. Rong and J. Zhang, *ACS Nano*, 2021, **15**, 2005–2037.
77 S. Gao, H. Lin, H. Zhang, H. Yao, Y. Chen and J. Shi, *Adv. Sci.*, 2019, **6**, 1801733.
78 S. Wang, Q. You, J. Wang, Y. Song, Y. Cheng, Y. Wang, S. Yang, L. Yang, P. Li, Q. Lu, M. Yu and N. Li, *Nanoscale*, 2019, **11**, 6270–6284.
79 J. Yu, F. Zhao, W. Gao, X. Yang, Y. Ju, L. Zhao, W. Guo, J. Xie, X. J. Liang, X. Tao, J. Li, Y. Ying, W. Li, J. Zheng, L. Qiao, S. Xiong, X. Mou, S. Che and Y. Hou, *ACS Nano*, 2019, **13**, 10002–10014.
80 C. Wu, X. Han, W. Feng, Z. Liu, L. Chen, B. Zhou, Y. Chen and J. Shi, *Chem. Eng. J.*, 2021, **411**, 128543.
81 Z. Wang, Y. Zhang, E. Ju, Z. Liu, F. Cao, Z. Chen, J. Ren and X. Qu, *Nat. Commun.*, 2018, **9**, 3334.
82 S. Zhang, Q. Li, N. Yang, Y. Shi, W. Ge, W. Wang, W. Huang, X. Song and X. Dong, *Adv. Funct. Mater.*, 2019, **29**, 1906805.
83 Q. You, K. Zhang, J. Liu, C. Liu, H. Wang, M. Wang, S. Ye, H. Gao, L. Lv, C. Wang, L. Zhu and Y. Yang, *Adv. Sci.*, 2020, **7**, 1903341.
84 M. Mao, X. Guan, F. Wu and L. Ma, *Nanomaterials*, 2022, **12**, 639.
85 X. Zhang, Y. Lu, Q. Chen and Y. Huang, *J. Mater. Chem. B*, 2020, **8**, 6459–6468.
86 S. Liu, L. Fang, H. Ding, Y. Zhang, W. Li, B. Liu, S. Dong, B. Tian, L. Feng and P. Yang, *ACS Nano*, 2022, **16**, 20805–20819.
87 R. André, F. Natálio, M. Humanes, J. Leppin, K. Heinze, R. Wever, H. C. Schröder, W. E. G. Müller and W. Tremel, *Adv. Funct. Mater.*, 2011, **21**, 501–509.

88 A. Y. Zhang, T. Lin, Y. Y. He and Y. X. Mou, *J. Hazard. Mater.*, 2016, **311**, 81–90.
89 S. Guan, X. Liu, Y. Fu, C. Li, J. Wang, Q. Mei, G. Deng, W. Zheng, Z. Wan and J. Lu, *J. Colloid Interface Sci.*, 2022, **608**, 344–354.
90 X. Zhu, M. Wang, H. Wang, Y. Ding, Y. Liu, Z. Fu, D. Lin, C. Lu and X. Tu, *Small*, 2022, **18**, 2204951.
91 C. Wu, S. Wang, J. Zhao, Y. Liu, Y. Zheng, Y. Luo, C. Ye, M. Huang and H. Chen, *Adv. Funct. Mater.*, 2019, **29**, 1901722.
92 L. H. Fu, Y. Wan, C. Qi, J. He, C. Li, C. Yang, H. Xu, J. Lin and P. Huang, *Adv. Mater.*, 2021, **33**, e2006892.
93 S. Gao, Y. Jin, K. Ge, Z. Li, H. Liu, X. Dai, Y. Zhang, S. Chen, X. Liang and J. Zhang, *Adv. Sci.*, 2019, **6**, 1902137.
94 X. Lu, S. Gao, H. Lin and J. Shi, *Small*, 2021, **17**, e2004467.
95 M. Chang, Z. Hou, M. Wang, C. Yang, R. Wang, F. Li, D. Liu, T. Peng, C. Li and J. Lin, *Angew Chem. Int. Ed. Engl.*, 2021, **60**, 12971–12979.
96 R. Zhang, B. Xue, Y. Tao, H. Zhao, Z. Zhang, X. Wang, X. Zhou, B. Jiang, Z. Yang, X. Yan and K. Fan, *Adv. Mater.*, 2022, **34**, e2205324.
97 D. Zhu, H. Chen, C. Huang, G. Li, X. Wang, W. Jiang and K. Fan, *Adv. Funct. Mater.*, 2022, **32**, 2110268.
98 Q. Zhang, S. Chen and H. Wang, *Green Chem.*, 2018, **20**, 4067–4074.
99 F. Cao, Y. Sang, C. Liu, F. Bai, L. Zheng, J. Ren and X. Qu, *ACS Nano*, 2022, **16**, 855–868.
100 D. Zhu, H. Chen, C. Huang, G. Li, X. Wang, W. Jiang and K. Fan, *Adv. Funct. Mater.*, 2022, **32**, 2110268.
101 Y. Bao, J. Chen, H. Qiu, C. Zhang, P. Huang, Z. Mao and W. Tong, *ACS Appl. Mater. Interfaces*, 2021, **13**, 24532–24542.
102 Y. Zhang, F. Wang, C. Liu, Z. Wang, L. Kang, Y. Huang, K. Dong, J. Ren and X. Qu, *ACS Nano*, 2018, **12**, 651–661.
103 M. Melchionna and P. Fornasiero, *Chem*, 2019, **5**, 1927–1928.
104 X. Lyu, X. Liu, C. Zhou, S. Duan, P. Xu, J. Dai, X. Chen, Y. Peng, D. Cui, J. Tang, X. Ma and W. Wang, *J. Am. Chem. Soc.*, 2021, **143**, 12154–12164.
105 Y. Ji, X. Lin, H. Zhang, Y. Wu, J. Li and Q. He, *Angew Chem. Int. Ed. Engl.*, 2019, **58**, 4184–4188.
106 G.-J. Cao, X. Jiang, H. Zhang, T. R. Croley and J.-J. Yin, *RSC Adv.*, 2017, **7**, 52210–52217.
107 H. Ye, J. Mohar, Q. Wang, M. Catalano, M. J. Kim and X. Xia, *Sci. Bull.*, 2016, **61**, 1739–1745.
108 C. Wei, Y. Liu, X. Zhu, X. Chen, Y. Zhou, G. Yuan, Y. Gong and J. Liu, *Biomaterials*, 2020, **238**, 119848.
109 T. Chen, G. Han and X. Li, *Bioact. Mater.*, 2022, **12**, 143–152.
110 J. M. Garcia-Martinez and E. P. Collar, *Polymers*, 2020, **13**, 86.
111 H. C. Zhou, J. R. Long and O. M. Yaghi, *Chem. Rev.*, 2012, **112**, 673–674.
112 Y. Wang, Y. Zhu, A. Binyam, M. Liu, Y. Wu and F. Li, *Biosens. Bioelectron.*, 2016, **86**, 432–438.
113 L. Zhang, S. S. Wan, C. X. Li, L. Xu, H. Cheng and X. Z. Zhang, *Nano Lett.*, 2018, **18**, 7609–7618.
114 O. Adegoke and P. B. Forbes, *Anal. Chim. Acta*, 2015, **862**, 1–13.
115 R. C. Castro, J. X. Soares, D. S. M. Ribeiro and J. L. M. Santos, *Sens. Actuators, B*, 2019, **296**, 126665.
116 J. Zhou, R. Zhao, Y. Du, S. Liu, W. Li, S. Gai, F. He, L. Feng and P. Yang, *Adv. Funct. Mater.*, 2022, **32**, 2112083.
117 H. Chen, K. Wen, J. Chen, W. Xing, X. Wu, Q. Shi, A. Peng and H. Huang, *Sci. Bull.*, 2020, **65**, 1580–1586.
118 X. Huang, J. Wang, H. Liu, T. Lan and J. Ren, *Talanta*, 2013, **106**, 79–84.
119 Z. Zhou, L. Yang, L. Huang, Y. Liao, Y. Liu and Q. Xiao, *Anal. Chim. Acta*, 2020, **1106**, 176–182.
120 X. Chen, T. Wang, W. Le, X. Huang, M. Gao, Q. Chen, S. Xu, D. Yin, Q. Fu, C. Shao, B. Chen and D. Shi, *Theranostics*, 2020, **10**, 3430–3450.
121 S. Wang, E. Zhou, X. Wei, R. Liu, C. Li, L. Pan, Y. Zheng and N. Xing, *ACS Omega*, 2022, **7**, 20241–20249.
122 R. Shen, P. Liu, Y. Zhang, Z. Yu, X. Chen, L. Zhou, B. Nie, A. Zaczek, J. Chen and J. Liu, *Anal. Chem.*, 2018, **90**, 4478–4484.
123 T. Zhou, Q. Yao, T. Zhao and X. Chen, *Talanta*, 2015, **141**, 80–85.
124 Q. Raas, F. E. Saih, C. Gondcaille, D. Trompier, Y. Hamon, V. Leoni, C. Caccia, B. Nasser, M. Jadot, F. Menetrier, G. Lizard, M. Cherkaoui-Malki, P. Andreoletti and S. Savary, *Biochim. Biophys. Acta, Mol. Cell Biol. Lipids*, 2019, **1864**, 567–576.
125 K. Zhang, C. Qi and K. Cai, *Adv. Mater.*, 2022, **35**, 2205409.
126 F. Wu, Q. Zhang, B. Sun, X. Chu, M. Zhang, Z. She, Z. Li, N. Zhou, J. Wang and A. Li, *J. Control Release.*, 2021, **338**, 46–55.
127 S. Bai, N. Yang, X. Wang, F. Gong, Z. Dong, Y. Gong, Z. Liu and L. Cheng, *ACS Nano*, 2020, **14**, 15119–15130.
128 X. Zhong, X. Wang, G. Zhan, Y. Tang, Y. Yao, Z. Dong, L. Hou, H. Zhao, S. Zeng, J. Hu, L. Cheng and X. Yang, *Nano Lett.*, 2019, **19**, 8234–8244.
129 G. Song, Y. Chen, C. Liang, X. Yi, J. Liu, X. Sun, S. Shen, K. Yang and Z. Liu, *Adv. Mater.*, 2016, **28**, 7143–7148.
130 X. Jing, F. Yang, C. Shao, K. Wei, M. Xie, H. Shen and Y. Shu, *Mol. Cancer*, 2019, **18**, 157.
131 Y. Li, L. Zhao and X. F. Li, *Technol. Cancer Res. Treat.*, 2021, **20**, 15330338211036304.
132 G. L. Wang, B. H. Jiang, E. A. Rue and G. L. Semenza, *Proc. Natl. Acad. Sci. U. S. A.*, 1995, **92**, 5510–5514.
133 Q. Chen, L. Feng, J. Liu, W. Zhu, Z. Dong, Y. Wu and Z. Liu, *Adv. Mater.*, 2016, **28**, 7129–7136.
134 N. Yang, W. Xiao, X. Song, W. Wang and X. Dong, *Nano-Micro Lett.*, 2020, **12**, 15.
135 Y. Wang, Y. Li, Z. Zhang, L. Wang, D. Wang and B. Z. Tang, *Adv. Mater.*, 2021, **33**, e2103748.
136 C. Yao, W. Wang, P. Wang, M. Zhao, X. Li and F. Zhang, *Adv. Mater.*, 2018, **30**, 1704833.
137 X. Wang, M. Wu, H. Li, J. Jiang, S. Zhou, W. Chen, C. Xie, X. Zhen and X. Jiang, *Advanced Science*, 2022, **9**, 2104125.
138 T. Wu, Y. Liu, Y. Cao and Z. Liu, *Adv. Mater.*, 2022, **34**, e2110364.

139 Q. Liu, L. Shi, Y. Liao, X. Cao, X. Liu, Y. Yu, Z. Wang, X. Lu and J. Wang, *Adv. Sci.*, 2022, **9**, e2200005.
140 P. Zhu, Y. Chen and J. Shi, *ACS Nano*, 2018, **12**, 3780–3795.
141 L. Gong, Y. Zhang, J. Zhao, Y. Zhang, K. Tu, L. Jiao, Q. Xu, M. Zhang and S. Han, *Small*, 2022, **18**, e2107656.
142 Z. Yang, Y. Luo, H. Yu, K. Liang, M. Wang, Q. Wang, B. Yin and H. Chen, *Adv. Mater.*, 2022, **34**, e2108908.
143 X. Zhou, M. You, F. Wang, Z. Wang, X. Gao, C. Jing, J. Liu, M. Guo, J. Li, A. Luo, H. Liu, Z. Liu and C. Chen, *Adv. Mater.*, 2021, **33**, e2100556.
144 W. Sun, Z. Zhou, G. Pratx, X. Chen and H. Chen, *Theranostics*, 2020, **10**, 1296–1318.
145 X. Song, J. Xu, C. Liang, Y. Chao, Q. Jin, C. Wang, M. Chen and Z. Liu, *Nano Lett.*, 2018, **18**, 6360–6368.
146 W. Zai, L. Kang, T. Dong, H. Wang, L. Yin, S. Gan, W. Lai, Y. Ding, Y. Hu and J. Wu, *ACS Nano*, 2021, **15**, 15381–15394.
147 T. Chanmee, P. Ontong, K. Konno and N. Itano, *Cancers*, 2014, **6**, 1670–1690.
148 Y. Wang, F. Gao, X. Li, G. Niu, Y. Yang, H. Li and Y. Jiang, *J. Nanobiotechnol.*, 2022, **20**, 69.
149 T. J. Zhou, Y. Xu, L. Xing, Y. Wang and H. L. Jiang, *Adv. Mater.*, 2021, **33**, e2100114.
150 P. Yang, J. Tao, F. Chen, Y. Chen, J. He, K. Shen, P. Zhao and Y. Li, *Small*, 2021, **17**, e2005865.
151 Z. Liu, T. Li, F. Han, Y. Wang, Y. Gan, J. Shi, T. Wang, M. L. Akhtar and Y. Li, *Biomater. Sci.*, 2019, **7**, 3683–3692.
152 D. Wang, J. Zhou, R. Chen, R. Shi, G. Xia, S. Zhou, Z. Liu, N. Zhang, H. Wang, Z. Guo and Q. Chen, *Biomaterials*, 2016, **107**, 88–101.
153 L. F. Yang, C. C. Ren, M. Xu, Y. L. Song, Q. L. Lu, Y. L. Wang, Y. Zhu, X. X. Wang and N. Li, *Nano Res.*, 2020, **13**, 2246–2258.
154 M. D. Liu, D. K. Guo, R. Y. Zeng, J. J. Ye, S. B. Wang, C. X. Li, Y. X. Sun, S. X. Cheng and X. Z. Zhang, *Adv. Funct. Mater.*, 2020, **30**, 2006098.
155 H. Z. Deng, Z. Yang, X. Y. Pang, C. Y. Zhao, J. Tian, Z. L. Wang and X. Y. Chen, *Nano Today*, 2022, **42**, 101337.
156 X. Y. Lu, S. S. Gao, H. Lin, L. D. Yu, Y. H. Han, P. A. Zhu, W. C. Bao, H. L. Yao, Y. Chen and J. L. Shi, *Adv. Mater.*, 2020, **32**, 2002246.
157 Z. Tang, P. Zhao, H. Wang, Y. Liu and W. Bu, *Chem. Rev.*, 2021, **121**, 1981–2019.
158 X. Chen, H. Zhang, M. Zhang, P. Zhao, R. Song, T. Gong, Y. Liu, X. He, K. Zhao and W. Bu, *Adv. Funct. Mater.*, 2019, **30**, 1908365.
159 L. S. Lin, J. B. Song, L. Song, K. M. Ke, Y. J. Liu, Z. J. Zhou, Z. Y. Shen, J. Li, Z. Yang, W. Tang, G. Niu, H. H. Yang and X. Y. Chen, *Angew. Chem., Int. Ed.*, 2018, **57**, 4902–4906.
160 L. H. Fu, C. Qi, Y. R. Hu, J. Lin and P. Huang, *Adv. Mater.*, 2019, **31**, e1808325.
161 B. Chen, K. Guo, X. Zhao, Z. Liu, C. Xu, N. Zhao and F. J. Xu, *Exploration*, 2023, 20220140.
162 A. L. Antaris, H. Chen, K. Cheng, Y. Sun, G. Hong, C. Qu, S. Diao, Z. Deng, X. Hu, B. Zhang, X. Zhang, O. K. Yaghi, Z. R. Alamparambil, X. Hong, Z. Cheng and H. Dai, *Nat. Mater.*, 2016, **15**, 235–242.
163 Y. Yu, B.-R. Xie, X.-H. Liu, J.-J. Ye, H. Cheng, Z. Zhong and X.-Z. Zhang, *J. Mater. Chem. B*, 2022, **10**, 1634–1640.
164 M. Ren, D. Dong, Q. Xu, J. Yin, S. Wang and F. Kong, *Talanta*, 2021, **234**, 122684.
165 M. Li, X. Huang and J. Ren, *Anal. Chem.*, 2021, **93**, 3042–3051.
166 J. Cao, B. Qiao, Y. Luo, C. Cheng, A. Yang, M. Wang, X. Yuan, K. Fan, M. Li and Z. Wang, *Biomater. Sci.*, 2020, **8**, 6561–6578.
167 W. Zhen, Y. Liu, W. Wang, M. Zhang, W. Hu, X. Jia, C. Wang and X. Jiang, *Angew Chem. Int. Ed. Engl.*, 2020, **59**, 9491–9497.
168 Q. Guan, L. Shi, C. Li, X. Gao, K. Wang, X. Liang, P. Li and X. Zhu, *ACS Biomater. Sci. Eng.*, 2019, **5**, 1023–1033.
169 K. Liu, H. Shang, X. Kong, M. Ren, J. Y. Wang, Y. Liu and W. Lin, *Biomaterials*, 2016, **100**, 162–171.
170 Y. Wang, S. Li, L. Feng, C. Nie, L. Liu, F. Lv and S. Wang, *ACS Appl. Mater. Interfaces*, 2015, **7**, 24110–24118.
171 D. H. Zhao, C. Q. Li, X. L. Hou, X. T. Xie, B. Zhang, G. Y. Wu, F. Jin, Y. D. Zhao and B. Liu, *ACS Appl. Mater. Interfaces*, 2021, **13**, 55780–55789.
172 X. Zhang, W. Wang, L. Su, X. Ge, J. Ye, C. Zhao, Y. He, H. Yang, J. Song and H. Duan, *Nano Lett.*, 2021, **21**, 2625–2633.
173 J. Weber, P. C. Beard and S. E. Bohndiek, *Nat. Methods*, 2016, **13**, 639–650.
174 Q. Fu, R. Zhu, J. Song, H. Yang and X. Chen, *Adv. Mater.*, 2019, **31**, e1805875.
175 E. Jung, J. Noh, C. Kang, D. Yoo, C. Song and D. Lee, *Biomaterials*, 2018, **179**, 175–185.
176 G. W. Kim, C. Kang, Y. B. Oh, M. H. Ko, J. H. Seo and D. Lee, *Theranostics*, 2017, **7**, 2463–2476.
177 T. Iwashita, S. Uemura, M. Shimizu, F. Hyodo, H. Tomita, R. Iwasaki, M. Takasu, T. Mori, H. Tanaka and M. Matsuo, *Ultrasound Med. Biol.*, 2019, **45**, 579–585.
178 E. Jung, C. Kang, J. Lee, D. Yoo, D. W. Hwang, D. Kim, S. C. Park, S. K. Lim, C. Song and D. Lee, *ACS Nano*, 2018, **12**, 392–401.
179 H. Chen, D. Zheng, W. Pan, X. Li, B. Lv, W. Gu, J. O. Machuki, J. Chen, W. Liang, K. Qin, J. Greven, F. Hildebrand, Z. Yu, X. Zhang and K. Guo, *ACS Appl. Mater. Interfaces*, 2021, **13**, 19710–19725.
180 Q. Wu, Q. Zhang, T. Yu, X. Wang, C. Jia, Z. Zhao and J. Zhao, *ACS Appl. Bio Mater.*, 2021, **4**, 4244–4253.
181 Y. Wang, J. Zhang, X. Lv, L. Wang, Z. Zhong, D. P. Yang, W. Si, T. Zhang and X. Dong, *Biomaterials*, 2020, **252**, 120111.
182 X. Li, H. Zhou, Z. Niu, K. Zheng, D. Niu, W. Zhao, X. Liu, W. Si, C. Li, P. Wang, J. Cao, Y. Li and G. Wen, *ACS Appl. Mater. Interfaces*, 2020, **12**, 24644–24654.
183 M. Tian, J. Sun, Y. Tang, B. Dong and W. Lin, *Anal. Chem.*, 2018, **90**, 998–1005.
184 D. Pan, A. H. Schmieder, S. A. Wickline and G. M. Lanza, *Tetrahedron*, 2011, **67**, 8431–8444.
185 Z. Yin, Q. Ji, D. Wu, Z. Li, M. Fan, H. Zhang, X. Zhao, A. Wu, L. Cheng and L. Zeng, *ACS Appl. Mater. Interfaces*, 2021, **13**, 14928–14937.

186 Y. Cheng, X. Tan, J. Wang, Y. Wang, Y. Song, Q. You, Q. Sun, L. Liu, S. Wang, F. Tan, J. Li and N. Li, *J. Control Release.*, 2018, **277**, 77–88.
187 Z. Wang, T. Jia, Q. Sun, Y. Kuang, B. Liu, M. Xu, H. Zhu, F. He, S. Gai and P. Yang, *Biomaterials*, 2020, **228**, 119569.
188 G. Taubes, *Science*, 2008, **321**, 356–361.
189 Y. Yang, X. Wu, L. Ma, C. He, S. Cao, Y. Long, J. Huang, R. D. Rodriguez, C. Cheng, C. Zhao and L. Qiu, *Adv. Mater.*, 2021, **33**, e2005477.
190 X. Zhou, Z. Wang, Y. K. Chan, Y. Yang, Z. Jiao, L. Li, J. Li, K. Liang and Y. Deng, *Adv. Funct. Mater.*, 2021, **32**, 2109469.
191 D. Sun, X. Pang, Y. Cheng, J. Ming, S. Xiang, C. Zhang, P. Lv, C. Chu, X. Chen, G. Liu and N. Zheng, *ACS Nano*, 2020, **14**, 2063–2076.
192 L. Lai, W. Zou, Y. Zhang, Y. Tu, S. Li, T. Xin, T. Zhou, S. Xu, P. Zheng, Q. Pan and W. Zhu, *Chem. Eng. J.*, 2022, **435**, 135084.
193 N. Yang, H. Guo, C. Cao, X. Wang, X. Song, W. Wang, D. Yang, L. Xi, X. Mou and X. Dong, *Biomaterials*, 2021, **275**, 120918.
194 Y. Shi, Y. Cao, J. Cheng, W. Yu, M. Liu, J. Yin, C. Huang, X. Liang, H. Zhou, H. Liu, Z. Yang, Y. Fang, H. Wei and G. Zhao, *Adv. Funct. Mater.*, 2022, **32**, 2111148.
195 L. Gao, Y. Liu, D. Kim, Y. Li, G. Hwang, P. C. Naha, D. P. Cormode and H. Koo, *Biomaterials*, 2016, **101**, 272–284.
196 K. Villa, J. Viktorova, J. Plutnar, T. Ruml, L. Hoang and M. Pumera, *Cell Rep. Phys. Sci.*, 2020, **1**, 100181.
197 K. Wang, Y. Sun, W. Xu, W. Zhang, F. Zhang, Y. Qi, Y. Zhang, Q. Zhou, B. Dong, C. Li, L. Wang and L. Xu, *Sens. Actuators, B*, 2022, **355**, 131298.
198 K. Wu, X. Wu, M. Chen, H. Wu, Y. Jiao and C. Zhou, *Chem. Eng. J.*, 2020, **387**, 124127.
199 J. Liu, L. Shi, Y. Wang, M. Li, C. Zhou, L. Zhang, C. Yao, Y. Yuan, D. Fu, Y. Deng, M. Liu, G. Wang, L. Wang and Z. Wang, *Nano Today*, 2022, **47**, 101627.
200 M. F. Chung, W. T. Chia, W. L. Wan, Y. J. Lin and H. W. Sung, *J. Am. Chem. Soc.*, 2015, **137**, 12462–12465.
201 Y. Cheng, J. Dai, C. Sun, R. Liu, T. Zhai, X. Lou and F. Xia, *Angew Chem. Int. Ed. Engl.*, 2018, **57**, 3123–3127.
202 R. Etzioni, N. Urban, S. Ramsey, M. McIntosh, S. Schwartz, B. Reid, J. Radich, G. Anderson and L. Hartwell, *Nat. Rev. Cancer*, 2003, **3**, 243–252.
203 X. Li, Y. Liu, X. Qi, S. Xiao, Z. Xu, Z. Yuan, Q. Liu, H. Li, S. Ma, T. Liu, Y. Huang, X. Zhang, X. Zhang, Z. Mao, G. Luo and J. Deng, *Adv. Mater.*, 2022, **34**, 2109004.
204 E. Jung, J. Noh, C. Kang, D. Yoo, C. Song and D. Lee, *Biomaterials*, 2018, **179**, 175–185.
205 M. Yu, B. S. Bouley, D. Xie, J. S. Enriquez and E. L. Que, *J. Am. Chem. Soc.*, 2018, **140**, 10546–10552.
206 L. Sun, J. Ouyang, F. Zeng and S. Wu, *Biomaterials*, 2022, **283**, 121468.
207 J. Chen, L. Chen, Y. Wu, Y. Fang, F. Zeng, S. Wu and Y. Zhao, *Nat. Commun.*, 2021, **12**, 6870.
208 M. Li, Y. Wang, X. Han, Y. Liu, M. Ma and L. Zhang, *Pharmaceutics*, 2022, **14**, 1988.
209 J. Ding, Y. Yao, J. Li, Y. Duan, J. R. Nakkala, X. Feng, W. Cao, Y. Wang, L. Hong, L. Shen, Z. Mao, Y. Zhu and C. Gao, *Small*, 2020, **16**, e2005038.
210 A. Jain, M. Behera, C. Mahapatra, N. R. Sundaresan and K. Chatterjee, *Mater. Sci. Eng. C*, 2021, **118**, 111416.
211 E. Jung, T. Kim, S. Bae, P. M. Kang and D. Lee, *Adv. Ther.*, 2021, **4**, 2000273.
212 W. Gao, X. Li, Z. Liu, W. Fu, Y. Sun, W. Cao, L. Tong and B. Tang, *Anal. Chem.*, 2019, **91**, 1150–1156.
213 C. Li, P. Wu, Y. Dou, Q. Li and J. Zhang, *View*, 2022, **3**, 20200137.
214 S. S. Virani, A. Alonso, H. J. Aparicio, E. J. Benjamin, M. S. Bittencourt, C. W. Callaway, A. P. Carson, A. M. Chamberlain, S. Cheng, F. N. Delling, M. S. V. Elkind, K. R. Evenson, J. F. Ferguson, D. K. Gupta, S. S. Khan, B. M. Kissela, K. L. Knutson, C. D. Lee, T. T. Lewis, J. Liu, M. S. Loop, P. L. Lutsey, J. Ma, J. Mackey, S. S. Martin, D. B. Matchar, M. E. Mussolino, S. D. Navaneethan, A. M. Perak, G. A. Roth, Z. Samad, G. M. Satou, E. B. Schroeder, S. H. Shah, C. M. Shay, A. Stokes, L. B. VanWagner, N. Y. Wang, C. W. Tsao, E. American Heart Association Council on, C. Prevention Statistics and S. Stroke Statistics, *Circulation*, 2021, **143**, e254–e743.
215 M. S. Oliveira, L. Y. Tanaka, E. L. Antonio, L. I. Brandizzi, A. J. Serra, L. Dos Santos, J. E. Krieger, F. R. M. Laurindo and P. J. F. Tucci, *Mol. Med. Rep.*, 2020, **21**, 1431–1438.
216 K. S. Cunningham, D. A. Spears and M. Care, *Forensic Sci. Res.*, 2019, **4**, 223–240.
217 R. Aikawa, T. Nagai, M. Tanaka, Y. Zou, T. Ishihara, H. Takano, H. Hasegawa, H. Akazawa, M. Mizukami, R. Nagai and I. Komuro, *Biochem. Biophys. Res. Commun.*, 2001, **289**, 901–907.
218 Z. Wang, H. Zhao, K. Chen, H. Li and M. Lan, *Anal. Chim. Acta*, 2021, **1188**, 339202.
219 J. Lee, L. Jeong, E. Jung, C. Ko, S. Seon, J. Noh and D. Lee, *J. Control Release.*, 2019, **304**, 164–172.
220 E. Jung, J. Lee, L. Jeong, S. Park, M. Lee, C. Song and D. Lee, *Biomaterials*, 2019, **192**, 282–291.
221 T. Y. Lee, W. J. Lu, C. A. Changou, Y. C. Hsiung, N. T. T. Trang, C. Y. Lee, T. H. Chang, T. Jayakumar, C. Y. Hsieh, C. H. Yang, C. C. Chang, R. J. Chen, J. R. Sheu and K. H. Lin, *Autophagy*, 2021, **17**, 4141–4158.
222 C. Cui, Z. Yang, X. Hu, J. Wu, K. Shou, H. Ma, C. Jian, Y. Zhao, B. Qi, X. Hu, A. Yu and Q. Fan, *ACS Nano*, 2017, **11**, 3298–3310.
223 Y. Zhao, R. Xie, N. Yodsanit, M. Ye, Y. Wang and S. Gong, *Nano Today*, 2020, **35**, 100986.
224 J. E. Freedman, *Arterioscler. Thromb. Vasc. Biol.*, 2008, **28**, s11–s16.
225 W. Gao, X. Li, Z. Liu, W. Fu, Y. Sun, W. Cao, L. Tong and B. Tang, *Anal. Chem.*, 2018, **91**, 1150–1156.
226 Y. Chen, Z. Chen, J. Duan, L. Gui, H. Li, X. Liang, X. Tian, K. Liu, Y. Li and J. Yang, *J. Nanobiotechnol.*, 2022, **20**, 145.
227 M. Zuo, W. Qian, Z. Xu, W. Shao, X. Y. Hu, D. Zhang, J. Jiang, X. Sun and L. Wang, *Small*, 2018, **14**, e1801942.

228 Q. Chen, J. Li, F. Han, Q. Meng, H. Wang, Q. Wei, Z. Li, F. Li, E. Xie, X. Qin, S. Chen, W. Wang, C. Liu, B. Li and F. Han, *Adv. Funct. Mater.*, 2022, **32**, 2201067.
229 G. Yang, M. Fan, J. Zhu, C. Ling, L. Wu, X. Zhang, M. Zhang, J. Li, Q. Yao, Z. Gu and X. Cai, *Biomaterials*, 2020, **255**, 120155.
230 A. Lin, Z. Sun, X. Xu, S. Zhao, J. Li, H. Sun, Q. Wang, Q. Jiang, H. Wei and D. Shi, *Nano Lett.*, 2022, **22**, 508–516.
231 D. Yoo, K. Guk, H. Kim, G. Khang, D. Wu and D. Lee, *Int. J. Pharm.*, 2013, **450**, 87–94.
232 H. Zhang, S. Li, Y. Liu, Y. Yu, S. Lin, Q. Wang, L. Miao, H. Wei and W. Sun, *Biomater. Sci.*, 2020, **8**, 5984–5993.
233 Y. Li, Q. Pan, J. Xu, X. He, H. A. Li, D. A. Oldridge, G. Li and L. Qin, *J. Orthop. Translat.*, 2021, **27**, 110–118.
234 J. Li, F. Han, J. Ma, H. Wang, J. Pan, G. Yang, H. Zhao, J. Zhao, J. Liu, Z. Liu and B. Li, *Adv. Funct. Mater.*, 2021, **32**, 2111208.
235 X. Mu, H. He, J. Wang, W. Long, Q. Li, H. Liu, Y. Gao, L. Ouyang, Q. Ren, S. Sun, J. Wang, J. Yang, Q. Liu, Y. Sun, C. Liu, X. D. Zhang and W. Hu, *Nano Lett.*, 2019, **19**, 4527–4534.
236 L. Lei, Q. Tu, L. Jiao, S. Xiang, L. Wang, X. Ran, B. Xiao, G. Feng, J. Feng and C. Zhang, *Chem. Eng. J.*, 2022, **432**, 134356.
237 L. Wu, X. Xiong, X. Wu, Y. Ye, Z. Jian, Z. Zhi and L. Gu, *Front. Mol. Neurosci.*, 2020, **13**, 28.
238 C. Li, Z. Zhao, Y. Luo, T. Ning, P. Liu, Q. Chen, Y. Chu, Q. Guo, Y. Zhang, W. Zhou, H. Chen, Z. Zhou, Y. Wang, B. Su, H. You, T. Zhang, X. Li, H. Song, C. Li, T. Sun and C. Jiang, *Adv. Sci.*, 2021, **8**, e2101526.
239 T. Kalogeris, C. P. Baines, M. Krenz and R. J. Korthuis, *Compr. Physiol.*, 2016, **7**, 113–170.
240 J. Wang, Y. Zhu, L. Yang, H. Liu, T. Zhou, F. Xu, P. Xu, L. Yuan and L. Liang, *ACS Sens.*, 2021, **6**, 1330–1338.
241 J. Yang, J. Yang, S. H. Liang, Y. Xu, A. Moore and C. Ran, *Sci. Rep.*, 2016, **6**, 35613.
242 L. Qiao, Y. Shen, S. Zhang, M. Wang, G. Lv, Q. Dou and C. Li, *BMEMat*, 2023, **1**, 12011.
243 M. Nita and A. Grzybowski, *Oxid. Med. Cell. Longev.*, 2016, **2016**, 3164734.
244 Y. Chen, G. Mehta and V. Vasiliou, *Ocul. Surf.*, 2009, **7**, 176–185.
245 S. W. Choi, B. G. Cha and J. Kim, *ACS Nano*, 2020, **14**, 2483–2496.